Australian Government
Department of Defence
Defence Science and
Technology Organisation

Composite Replacement Panel Strain Survey – Test results and data analysis

Paul J. Callus

Air Vehicles Division
Platforms Sciences Laboratory

DSTO-TR-1701

ABSTRACT

DSTO, in collaboration with the Cooperative Research Centre for Advanced Composite Structures, produced a demonstrator Composite Replacement Panel (CRP) as a replacement for F-111C Panel 3208 (Part Number 12B-3913). As part of the airworthiness certification program for the CRP technology, the demonstrator CRP, in the Composite Replacement Panel Strain Survey (CRPSS), was installed on a Royal Australian Air Force F-111C aircraft prior to a Cold Proof Load Test (CPLT). Strains in the CRP and local sub-structure were recorded as the aircraft was cooled from ambient to –40 °C. The magnitude of these thermally induced strains were moderate and lower on the side of the aircraft containing the CRP, implying that installing CRPs may reduce load in airframe sub-structures. The strain gauge measurements during the CPLT were compared with predictions made using the F-111C Internal Loads Finite Element Model and associated sub-models. The response of most strain gauges were predicted with reasonable accuracy although the strains in skin panels were not predicted well. Modification of the sub-models would be required to predict accurately the strains in all CRPSS gauges.

Published by

DSTO Platforms Sciences Laboratory
506 Lorimer St
Fishermans Bend, Victoria 3207 Australia

Telephone: (03) 9626 7000
Fax: (03) 9626 7999

AR-013-373
April 2005

APPROVED FOR PUBLIC RELEASE

Composite Replacement Panel Strain Survey – Test results and data analysis

Executive Summary

The Defence Science and Technology Organisation (DSTO), in collaboration with the Cooperative Research Centre for Advanced Composite Structures (CRC-ACS), is developing the Composite Replacement Panel Technology (CRPT). The aim of this technology is to provide the Australian Defence Force with an alternative for the through-life-support of structural, bonded metallic, aircraft panels. A demonstrator CRP has been designed and manufactured as a replacement for F-111C Panel 3208 (Part Number 12B-3913), an outboard nacelle panel located on the right hand side of the aircraft between Fuselage Stations 496 and 531.

Many existing bonded panels are expensive to support because the materials, pre-bonding surface treatments and thin skins used in their construction make them susceptible to damage from corrosion, fatigue, disbonding and impact. The CRPT approach will be to replace such panels with those constructed from advanced composite materials.

Two of the airworthiness certification requirements for the CRPT are demonstration that (i) CRPs do not induce adverse thermal strains into the airframe, and (ii) the capability exists to predict strain within CRPs and the aircraft sub-structure under the combined action of thermal and mechanical loading. Much of the data necessary for this demonstration was obtained in the Composite Replacement Panel Strain Survey (CRPSS), conducted at Royal Australian Air Force (RAAF) Base Amberley in June 2004. The CRPSS consisted of the instrumented demonstrator CRP installed on an instrumented F-111C undergoing a Cold Proof Load Test (CPLT). Strains were measured both as the aircraft was cooled from ambient to the CPLT test temperature of –40 °C and for each of the four CPLT loadcases.

Strains, other than simple thermal contraction, were generated during cool-down because the airframe was constructed from materials with differing coefficients of thermal expansion (CTEs). The strains were moderate, up to approximately 450 με at –40 °C, and the difference between the sides of the aircraft with the CRP and the opposite side was typically less than 50 με. The absolute magnitude of strains in the sub-structure were lower on the side that contained the CRP. If this result applies also at elevated temperatures then it may be concluded that incorporating CRPs into metallic airframes would not induce adverse loads into the sub-structure. Further analysis and testing is required to determine whether this is the case.

The strain gauge measurements from the CRPSS were compared to predictions made using the December 2002 version of the F-111C Internal Loads Finite Element Model (ILM) and associated fine grid sub-models. Most gauges were predicted with reasonable accuracy although the strains in skin panels and one structural component were not predicted well. Modification of the sub-models would be required to predict accurately the CRPSS results and thus the combined effect of non-ambient temperature and applied mechanical load on strains in a metallic airframe containing a CRP.

Author

Paul J. Callus
Air Vehicles Division

Dr Paul Callus gained his PhD from Monash University in 1993. He worked with CSIRO for four years developing electrode coatings for ceramic fuel cells. He then spent two years at RMIT investigating failure processes in textile composites. He is currently a Senior Research Scientist in the Composites and Low Observables Functional Area of the Air Vehicles Division. He has worked on development of composite replacement panels and the certification of composite structure. His current focus is to apply this technology in the development of multifunctional aircraft structure.

Contents

1. Introduction

1.1 Background

There is increasing pressure on aircraft operators, including the Australian Defence Force, to reduce the through-life-support costs for their fleets. A critical aspect of this is the maintenance and repair of airframes. Most aircraft contain metallic structural panels, many of which are of bonded metallic honeycomb construction. Although these panels are structurally efficient (lightweight and stiff), they are often expensive to maintain because the materials, pre-bonding surface treatments and thin skins used in their construction make them susceptible to damage from corrosion, fatigue, disbonding and impact. Panels need to be replaced once the relatively tight repair limits have been exceeded.

An alternative to direct replacement is to substitute bonded metallic panels with panels that have been manufactured from advanced composite materials. Composites are not susceptible to fatigue and corrosion damage, and can be designed in a more robust configuration than the panels they replace.

The Defence Science and Technology Organisation (DSTO), in collaboration with the Cooperative Research Centre for Advanced Composite Structures (CRC-ACS), is developing the capability to replace metallic aircraft panels. This is known as the Composite Replacement Panel Technology (CRPT).

The Composite Replacement Panels (CRPs) would be significantly more durable than the existing metallic (aluminium) panels because the materials and construction would be resistant to corrosion, fatigue and impact as described above. Manufacturing costs would be competitive because low temperature composite materials would be used. These composites may be cured in an oven under vacuum pressure only, they would not require the expensive tooling and autoclave curing required for traditional aerospace composites. Finally, certification costs would be low because the CRPT itself would be certified. For any specific panel only those aspects that were different from the approved set of design solutions would need to be tested.

Two of the airworthiness certification requirements for the CRPT are demonstration that (i) CRPs do not induce adverse thermal strains into the airframe, and (ii) the capability exists to predict strain within CRPs and the aircraft sub-structure under the combined action of thermal and mechanical loading. Much of the experimental data necessary for this demonstration was obtained in the Composite Replacement Panel Strain Survey (CRPSS). This report presents the results and analysis from the CRPSS.

1.2 Composite Replacement Panel Strain Survey (CRPSS)

The aims of the CRPSS were to:

(i) demonstrate that CRPs do not induce adverse loads into aircraft sub-structure at sub-ambient temperature, and

(ii) provide the experimental data to validate the finite element (FE) modelling approach used in the design of the demonstrator CRP.

Aim (i) was required because the coefficient of thermal expansion (CTE) of materials and geometry (hat stiffened versus honeycomb stiffened skins) are different for CRPs and the existing metallic panels. There is a possibility that this difference will create adverse loads within the sub-structure when the aircraft is subjected to non-ambient temperatures.

Aim (ii) required that the FE modelling used to design the CRPs be shown to predict, with sufficient accuracy, the strains within CRPs and the surrounding sub-structure. This would validate the design-by-analysis approach and allow future CRPs to be designed without the need for full-scale testing.

These aims would normally be demonstrated by conducting a full-scale test on a CRP using representative loading, then comparing the predicted and measured strains. However the costs of such a test were prohibitive. Fortunately an alternative was available for this demonstrator, the F-111 Cold Proof Load Test (CPLT).

The CPLT is part of the safety-by-inspection management regime for the F—111 aircraft. It is a proof test designed to load critical D6ac steel components of the airframe to their Design Limit Load (DLL). The critical crack size required to cause catastrophic failure in D6ac steel falls with temperature. The CPLT is therefore conducted at -40 °C so that, if the D6ac components survive the CPLT then it can be assumed that the cracks within the components must be sufficiently small that they will not grow to a critical length prior to the next CPLT.

If an instrumented CRP were installed on a F-111 aircraft during a CPLT the CRP would certainly experience sub-ambient temperatures (thereby providing data to satisfy part of aim (i) above) and, depending on the location of the panel, could also experience significant mechanical loads (thereby providing data to satisfy aim (ii)).

A demonstrator Composite Replacement Panel (CRP) had been designed and manufactured as a replacement for F-111C Panel 3208 (General Dynamics Part Number 12B-3913). This panel is located on the right hand outboard engine nacelle, between Fuselage Stations (FS) 496 and FS 531, and fastened to the sub-structure with 130 screws [1]. It is approximately 890 mm long x 1180 mm high with moderate curvature about the aircraft longitudinal axis and slight curvature about the aircraft normal. The Part Number for the demonstrator CRP is CRC-ACS-511b-PN-001, however it has been referred to in previous documents as Panel I. The referred name of Panel I shall also be used through this document.

The CPLT would not impart the critical loading condition for Panel 3208, however it was judged that sufficient load should be imparted into the panel to validate the FE modelling.

In addition, the well-defined load and temperature conditions of the CPLT were expected to ease greatly the interpretation of strain gauge data.

An additional factor that eased significantly the prediction and interpretation of strain gauge data was availability of the F-111C Internal Loads Model (ILM). The ILM is a FE model that predicts accurately the load distribution in the F-111C sub-structure for any given CPLT or flight condition. The ILM was developed under contract by Lockheed Martin Tactical Aircraft Systems (Lockheed) through the F-111 Sole Operator Program in cooperation with Australian industry and DSTO engineers.

The ILM was validated by correlating its predictions with data from the F-111C Fuselage Strain Survey (FSS). The FSS was conducted from July to October 2002. In that program a RAAF F-111C (A8-144) was instrumented with approximately 470 strain gauges and a number of strain surveys, including a full CPLT, were conducted.

2. Method

2.1 CRPSS

The CRPSS was conducted on 29 June 2004 in accordance with the test plan [2]. Aircraft A8-143 was used and the following steps were performed:

a. removal of the existing Panels 3208 and 3108 (same position as Panel 3208 but on opposite side of aircraft) from the F-111C,
b. installation of strain gauges to the sub-structure beneath Panels 3208 and 3108,
c. installation of Panels I and 3108,
d. installation of strain gauges to Panels I and 3108,
e. connection of all strain gauges to the data acquisition system,
f. acquisition of data during (i) cool-down from ambient temperature to –40 °C, and (ii) each CPLT loadcase,
g. removal of Panels I and 3108 after the aircraft had returned to room temperature and the CPLT chamber opened,
h. removal of strain gauges from the sub-structure and Panel 3108 then restoration of the surfaces,
i. installation of the original metallic panels (Panel 3208 and 3108).

All data channels functioned correctly throughout the test and the data was supplied by the data acquisition contractor. Figure 1 shows photographs of the installed Panel I and Figure 2 is a photograph of the aircraft during CPLT loading.

(a)

(b)

Figure 1: (a) Overall and (b) close-up views of Panel I installed on A8-143 prior to the CRPSS

Figure 2: Photograph of A8-143 during the CRPSS

2.2 FE modelling

A structural analysis of the CRPSS using the ILM was reported in reference [1]. In summary, FE modelling was used to predict the stresses, strains, fastener loads and stability modes in Panel I and the local sub-structure for the four CPLT load cases.

The ILM was developed to provide the internal structural loads for future fine grid finite element models. As such, the mesh detail was intentionally coarse and only sufficient to provide representative load transfer. Refinement of the mesh was required for any analysis that required stress and strain output. Thus, in reference [1], the ILM was used in conjunction with a series of fine-grid sub-models. Broadly, the grid point displacements and rotations for the entire aircraft during CPLT loading were predicted using the ILM. These results were then input into a more refined sub-model of the panel and surrounding structure to more accurately predict the panel stresses, strains and stability modes.

Various modifications were made to the ILM in order to enable its use in this application. These included the addition of capability to measure the thermal residual internal loads distribution and also the incorporation of composite laminate material properties for Panel I.

The ILM used for the analysis in reference [1] and this report, was up to date in accordance with the concurrent version control software as of 2 December 2002 (ILMr1). The ILM was subsequently revised a number of times as a result of correlation with the FSS. An analysis using the first of these revised versions (F111C Revision 2 Internal Load Model (ILMr2i2) released on 21 October 2003) was presented in reference [1]. It showed that the revision had very little effect on the CRPSS predictions.

More recently a report has been released that describes the correlation of the ILM with the data from the FSS and further revisions to the ILM [3]. Substantial effort would be required to rework the analysis described in reference [1], conducted using ILMr1, with the version of the ILM current at the time of preparing this report (September-December 2004). Resource constraints prevented this rework, therefore the predictions made in reference [1] are used in this report.

2.3 Data analysis

Experimental and predicted strains for each of the locations gauged in the CRPSS were obtained by; identifying the element number corresponding to the gauge location, identifying the surface of the element on which the gauge was bonded, identifying the gauge type, identifying the gauge alignment, extracting the predicted strain from the ILM, transforming the predicted strains from material to gauge axes, extracting the measured CRPSS strains, and extracting FSS strains for those locations when there was a FSS gauge at the same position. These processes are detailed in Appendix A.

The strain for each CRPSS gauge was plotted against temperature for the cool-down so that the effect of thermal changes could be assessed. Strain was also plotted against consolidated load level for the CPLT loadcases. A variety of comparisons were made so that the data could be validated and the ILM predictions assessed. The comparisons were; CRPSS left hand side compared to right hand side, CRPSS gauges compared to FSS gauges, FSS compared to ILM predictions for FSS, CRPSS compared to ILM predictions for FSS and finally CRPSS compared to ILMr1 predictions for CRPSS.

3. Results and Discussion

3.1 Strain gauge locations

The positions of strain gauges for the CRPSS are shown in Figure 3 and details summarised in Table 1. These strain gauge locations were chosen because they corresponded to the position of gauges on Panel 3208 and the adjoining sub-structure that were used in the FSS. Matching the gauge positions from these two tests would facilitate comparisons that could be used to validate data and gain insight into the behaviour of the structure.

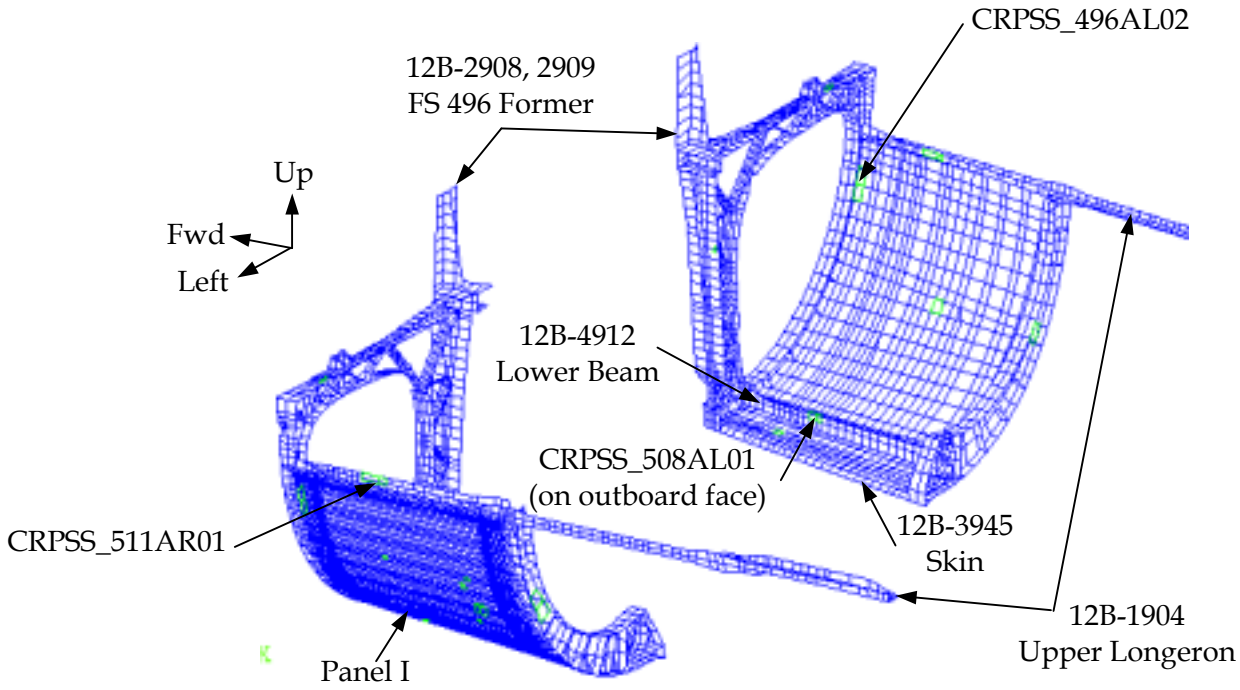

View from upper aft left looking inboard and down

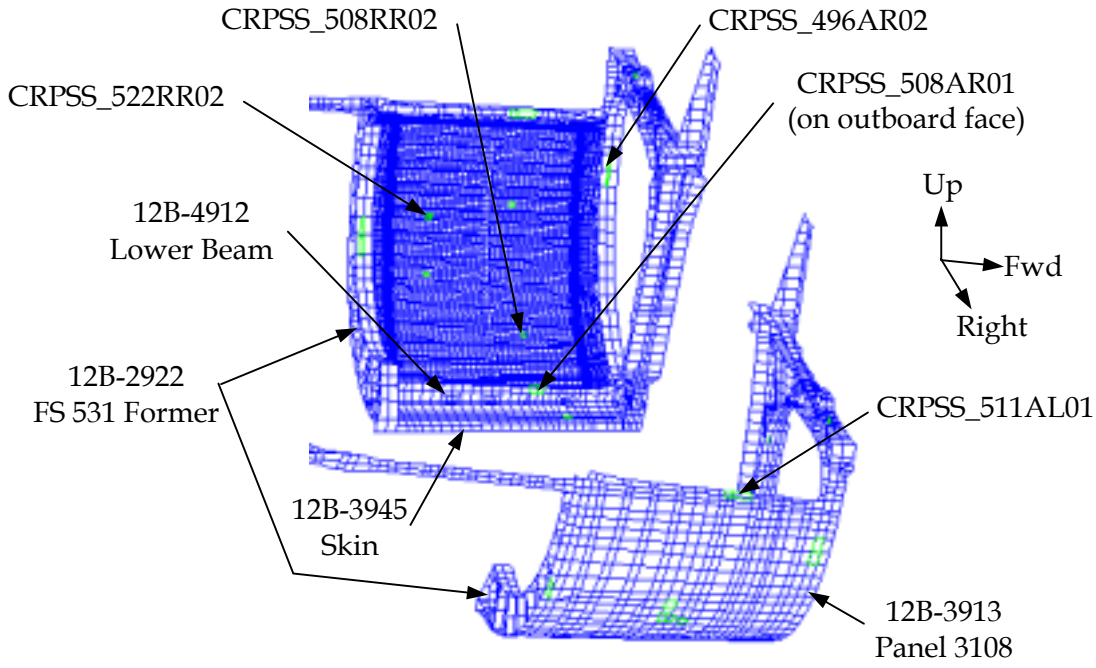

View from upper aft right looking inboard and down

Figure 3: Various views of ILMr1 showing the components and locations of strain gauges. All gauge locations are highlighted on all figures but only visible gauges are labelled. Continued overleaf...

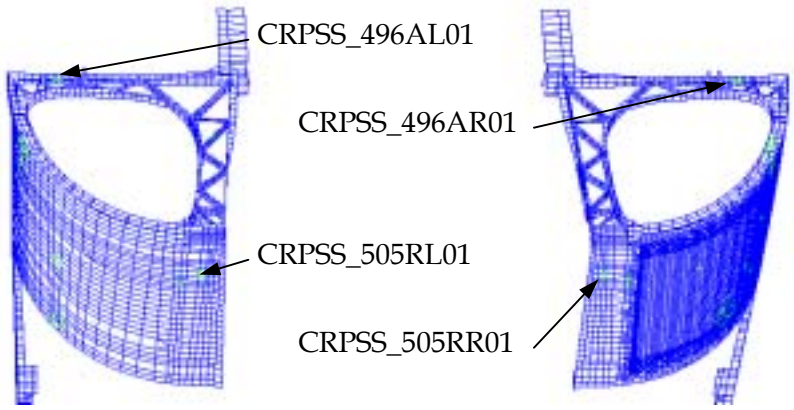

View from lower forward looking up and aft

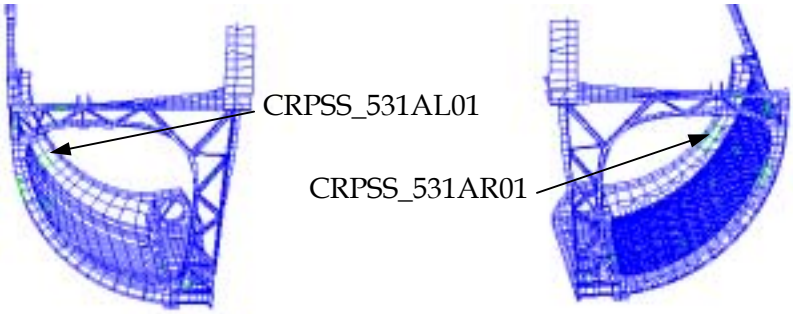

View from upper forward looking aft and down

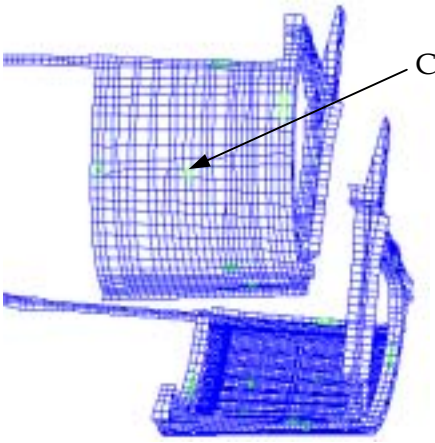

View from lower forward
right looking inboard and up

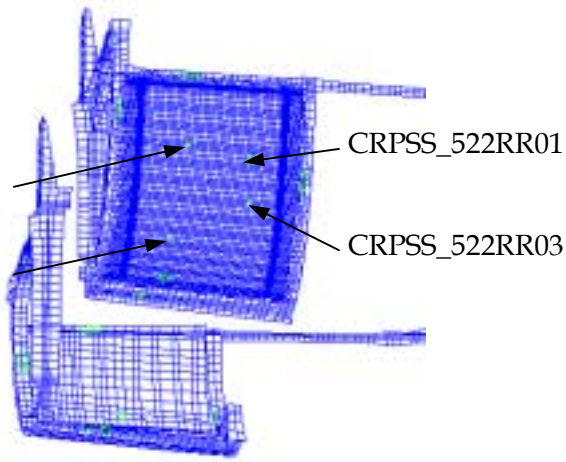

View from lower forward
left looking inboard and up

…continued. *Figure 3: Various views of ILMr1 showing the components and locations of strain gauges. All gauge locations are highlighted on all figures but only visible gauges are labelled*

Table 1: Strain gauge details

Channel	CRPSS		Location	FSS		Orientation[1]	MCID[2]	Loc. on element	Alignment (°)		
	Gauge ID	Element		Gauge ID	Element				αa	αb	αc
1	CRPSS_496AL01	406406 406407	12B-290[8,9] FS496 Former	C496AL38	456406 456407	u	400200	mid	0.0		
2	CRPSS_496AR01	456406 456407		Not installed		u	400200	mid	0.0		
3	CRPSS_496AL02	405102 405103		C496AL35	455181 455182	u	400300	Z2	0.0		
4	CRPSS_496AR02	455171 455172		Not installed		u	400300	Z2	0.0		
5-7	CRPSS_505RL01	415381	12B-3945 Skin	C505RL01	465381	cba	400100	Z1	180.0	135.0	90.0
8-10	CRPSS_505RR01	465355		Not installed		abc	400100	Z1	180.0	-135.0	-90.0
11	CRPSS_508AL01	416176 416177	12B-4912 Lower Beam	C508AL02	466176 466177	u	400100	Z1	-2.0		
12	CRPSS_508AR01	466176 466177		C508AR02	416176 416177	u	400100	Z1	178.0		
13	CRPSS_511AL01	409124 409129	12B-1904 Upper Long.	C510AL03	459124 459129	u	400100	Z1	0.0		
14	CRPSS_511AR01	459124 459129		C510AR03	409124 409129	u	400100	Z1	0.0		
15-17	CRPSS_514RL01	413880	12B-3913 Panel 3108	C514RL01	463903 463904 463926 463927	cba	400100	Z1	-90.0	135.0	180.0
18	CRPSS_531AL01	406718 406719	12B-2922 FS531 Former	C531AL05	456718 456719	u	400300	Z1	30.7		
19	CRPSS_531AR01	456716 456717		Not installed		u	400300	Z1	147.1		
20-22	CRPSS_508RR01	1952727	Fwd Lwr Skin Opp. Cap	Not installed		cba	2881104	Layer 1	0.0	-45.0	-90.0
23-25	CRPSS_508RR02	1957496	Fwd Lwr Hat Cap	Not installed		cba	2881104	Layer 1	0.0	-45.0	-90.0
26-28	CRPSS_509RR01	1952897	Fwd Uppr Skin	Not installed		cba	2881104	Layer 1	0.0	-45.0	-90.0
29-31	CRPSS_522RR01	1954243	Aft Uppr Skin Opp. Cap	Not installed		cba	2881104	Layer 1	0.0	-45.0	-90.0
32-34	CRPSS_522RR02	1956925	Aft Uppr Hat Cap	Not installed		cba	2881104	Layer 1	0.0	-45.0	-90.0
35-37	CRPSS_522RR03	1954231	Aft Lwr Skin	Not installed		cba	2881104	Layer 1	0.0	-45.0	-90.0

1 u: unidirectional, abc or cba: rosette with orientation as described in Section A.3

2 Material Coordinate Identification

The location of Panel I in the FE models used in reference [1] was on the opposite side of the aircraft to that of Panel I during the CRPSS. That is, Panel I was located on the right hand side of the aircraft (starboard) however it was modelled on the left hand side (port) of ILMr1. The elements for the CRPSS gauges were therefore determined by identifying the element(s) on the ILMr1 model that corresponded to the actual gauge position, but the corresponding element on the opposite side of the model was used. For example, CRPSS_496AL01 was an axial strain gauge located on the left hand side of the FS 496 former. The elements corresponding to this location were 456406 and 456407. These were on the left hand side of ILMr1. The elements that were used for strain predictions in this report were the corresponding elements on the right hand side of the aircraft, 406406 and 406407.

3.2 Effect of temperature

3.2.1 Temperature compensation

The effect of sub-ambient temperature was established by recording all strain gauges during the cool-down of aircraft from room temperature to –40 °C immediately prior to the CRPSS. The strains recorded by each of the CRPSS strain gauges was temperature compensated because the coefficient of thermal expansion (CTE) of these gauges did not match precisely the CTE of the material on which they were bonded. The temperature compensation relations were established using either experimental data or the relations shown on the corresponding strain gauge Engineering Data Sheets [5].

Experimental data was obtained for CEA-06-062UW-350 strain gauges bonded to D6ac and N32-FA-5-350-11 strain gauges bonded to MTM49-3 composite. Reference specimens with both of these gauge/material combinations were located near the aircraft in the CPLT chamber and the strains recorded at the same time as the cool-down and CRPSS. This data was plotted and a fourth order regression performed through each set. The resulting temperature compensation curves were expressed as fourth order polynomials to maintain consistency with the strain gauge Engineering Data Sheets.

Figure 4 shows the relations for the strain gauge/material combinations described in Table 2. The temperature compensation relations are shown as Equations (1) to (6).

$$\text{Thermal strain (CEA-06-062UW-350 on D6ac) } (\mu\varepsilon) = 9.82\text{E-}06\ T^4 + 8.91\text{E-}04\ T^3 - 8.49\text{E-}02\ T^2 + 3.55\text{E+}00\ T - 4.37\text{E+}01 \quad (1)$$

$$\text{Thermal strain (CEA-06-062UW-350 on aluminium) } (\mu\varepsilon) = -4.97\text{E-}07\ T^4 + 4.13\text{E-}04\ T^3 - 8.33\text{E-}02\ T^2 + 4.48\text{E+}00\ T - 6.35\text{E+}01 \quad (2)$$

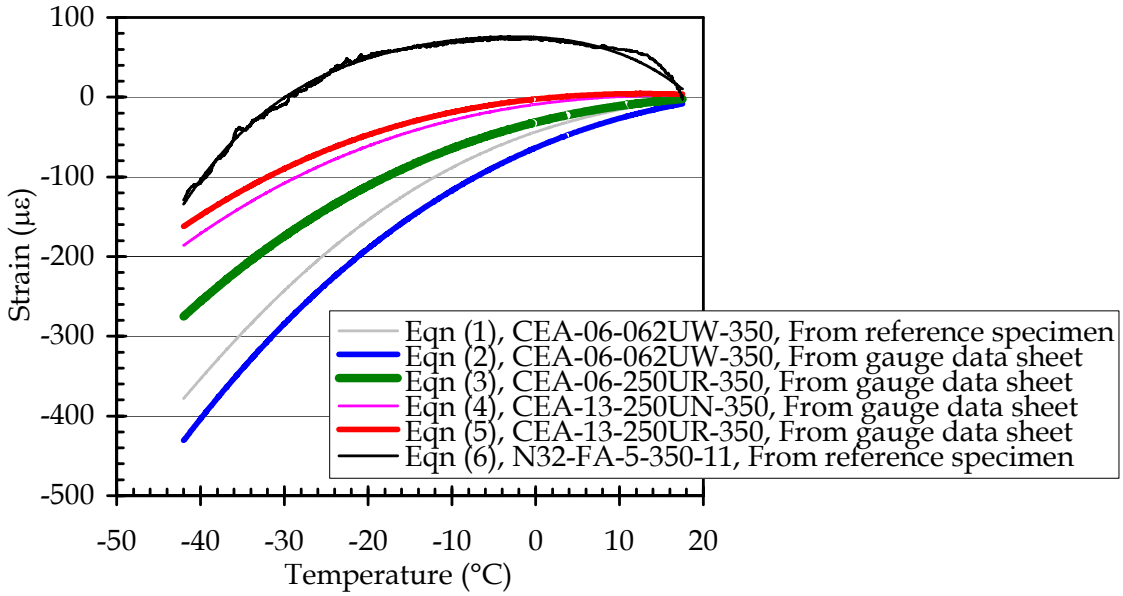

Figure 4: Temperature compensation curves for the strain gauges used in the CRPSS

Thermal strain (CEA-06-250UR-350 on D6ac) (με) =
$-3.97E\text{-}07\ T^4 + 3.30E\text{-}04\ T^3 - 6.08E\text{-}02\ T^2 + 2.63E+00\ T - 3.16E+01$ (3)

Thermal strain (CEA-13-250UN-350 on aluminium) (με) =
$-3.81E\text{-}07\ T^4 + 3.24E\text{-}04\ T^3 - 5.15E\text{-}02\ T^2 + 1.45E+00\ T - 9.05E+00$ (4)

Thermal strain (CEA-13-250UR-350 on aluminium) (με) =
$-3.90E\text{-}07\ T^4 + 3.23E\text{-}04\ T^3 - 4.96E\text{-}02\ T^2 + 1.12E+00\ T - 2.49E+00$ (5)

Thermal strain (N32-FA-5-350-11 on MTM49-3) (με) =
$-6.77E\text{-}05\ T^4 - 2.46E\text{-}03\ T^3 - 1.16E\text{-}01\ T^2 - 5.66E\text{-}01\ T + 7.51E+01$ (6)

3.2.2 Thermal effects

3.2.2.1 Sub-structure

For each of the CRPSS gauges the strain from the temperature compensation equation specified in Table 2 was subtracted from the strain measured during cool-down. For the sub-structure the resulting strains are plotted in Figure 5.

In all components except for the FS 531 Former the strains on the left and right hand side of the aircraft sub-structure followed the same trends, with the absolute strains on the left being larger than those on the right. The difference was less than 50 με for all locations except the lower beam (197 με) and the FS 531 Former (177 με compression on left hand side and 16 με tension on the right hand side). All of these differences occurred over absolute thermal strains ranging up to 460 με.

Table 2: Details for temperature compensation calculations

Channel	CRPSS strain gauge	Location	Material	Gauge type	T compensation equation number
1	CRPSS_496AL01	12B-290[8,9] FS496 Former	D6ac steel	CEA-06-062UW-350	1
2	CRPSS_496AR01				
3	CRPSS_496AL02				
4	CRPSS_496AR02				
5-7	CRPSS_505RL01	12B-3945 Skin	D6ac steel	CEA-06-250UR-350	3
8-10	CRPSS_505RR01				
11	CRPSS_508AL01	12B-4912 Lower Beam	D6ac steel	CEA-06-062UW-350	1
12	CRPSS_508AR01				
13	CRPSS_511AL01	12B-1904 Upper Long.	2024-T851 aluminium	CEA-06-062UW-350	2
14	CRPSS_511AR01				
15-17	CRPSS_514RL01	12B-3913 Panel 3108	2024-T851 aluminium	CEA-13-250UR-350	5
18	CRPSS_531AL01	12B-2922 FS531 Former	2024-T851 aluminium	CEA-13-250UN-350	4
19	CRPSS_531AR01				
20-22	CRPSS_508RR01	Panel I	MTM49-3 composite	N32-FA-5-350-11	6
23-25	CRPSS_508RR02				
26-28	CRPSS_509RR01				
29-31	CRPSS_522RR01				
32-34	CRPSS_522RR02				
35-37	CRPSS_522RR03				
-	Reference gauges	D6ac ref.	D6ac	CEA-06-062UW-350	1
-		MTM49-3 ref.	MTM49-3	N32-FA-5-350-11	6

The absolute differences between many of the gauges was relatively small, however so was the absolute strain. Thus the percentage differences for half of the gauges were quite large, peaking in Leg A (Figure A2) of the 12B-3945 skins with a 500 % difference. However this was clearly artificial given that the gauge on the left hand side recorded 1 με and the right gauge recorded –4 με. A difference of 5 με in the strain between the left and right hand side of an aircraft could hardly be judged as significant.

The issue of moderate absolute, but large percentage, differences was addressed in reference [3] by using a fixed strain deviation band (strain magnitude) rather than a percentage difference. Reference [3] stated that it was originally intended to consider that a difference of ±15 % between the ILM prediction and FSS data represented a good correlation. However it was found that the percentage difference approach placed too much significance on the low strains, where acceptable absolute differences may produce large percentage differences. The fixed strain deviation band was the 99.9 %

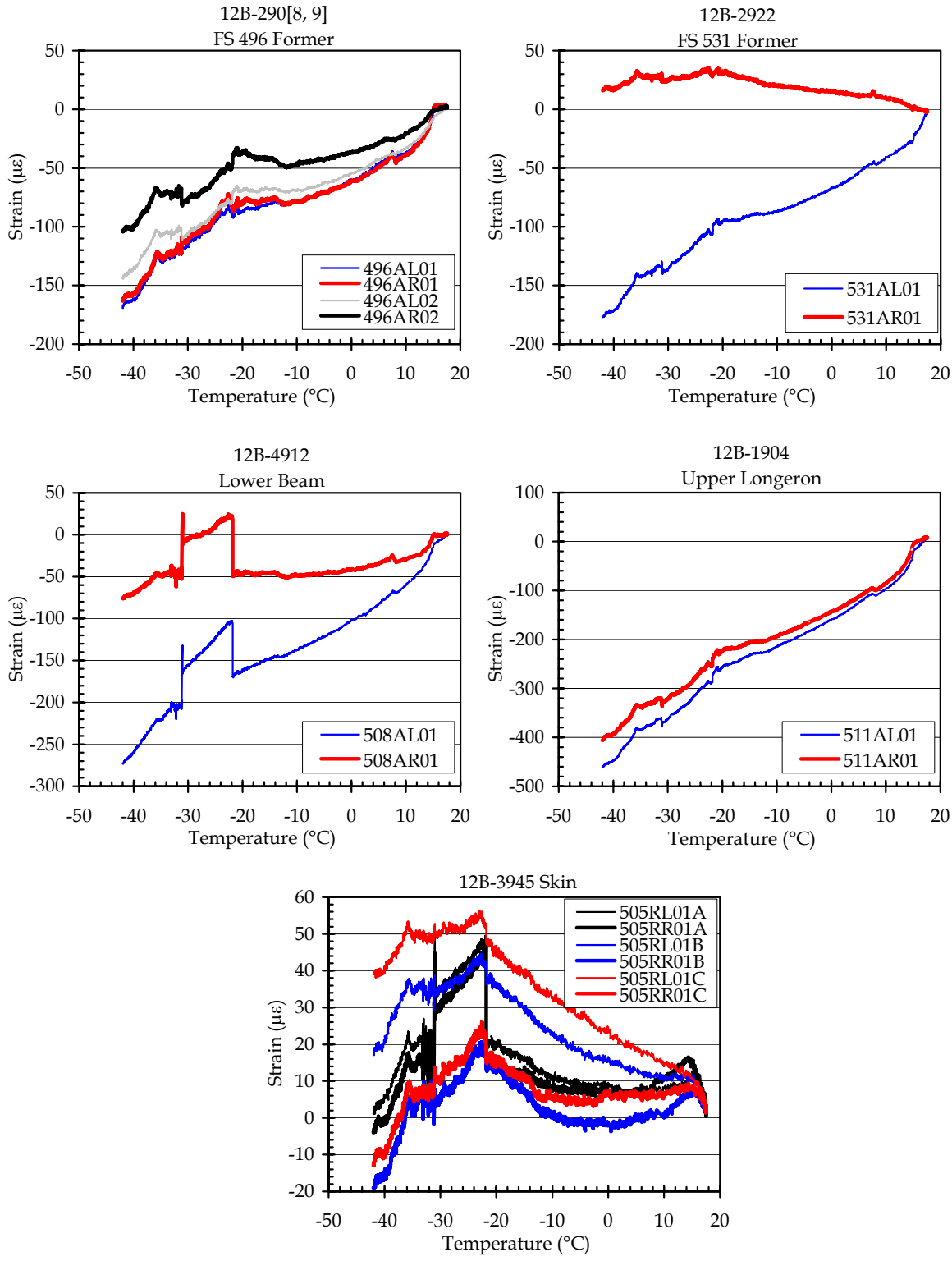

Figure 5: The effect of temperature on strain in the sub-structure. The A, B and C in the 505RX01[A, B, C] gauges refer to the Legs of the strain gauge rosettes

probability band for all gauges and loadcases and was calculated as ±363.5 με for the FSS. Only those differences larger than this band, on critical components, were investigated further in reference [3].

3.2.2.2 Panels 3108 and I

The temperature compensated strains measured during cool-down for Panels 3108 and I are plotted in Figure 6. The strains in Panel I should not be compared strictly to those in Panel 3108 because these panels were constructed from different materials in a different geometry. However it is useful to make some observations. Firstly the trends in axial strains matched well, including a step of approximately 20 με in the range –22 to –31 °C. In contrast, the strains in Legs B and C were opposite, compression in Panel 3108 and tension in Panel I.

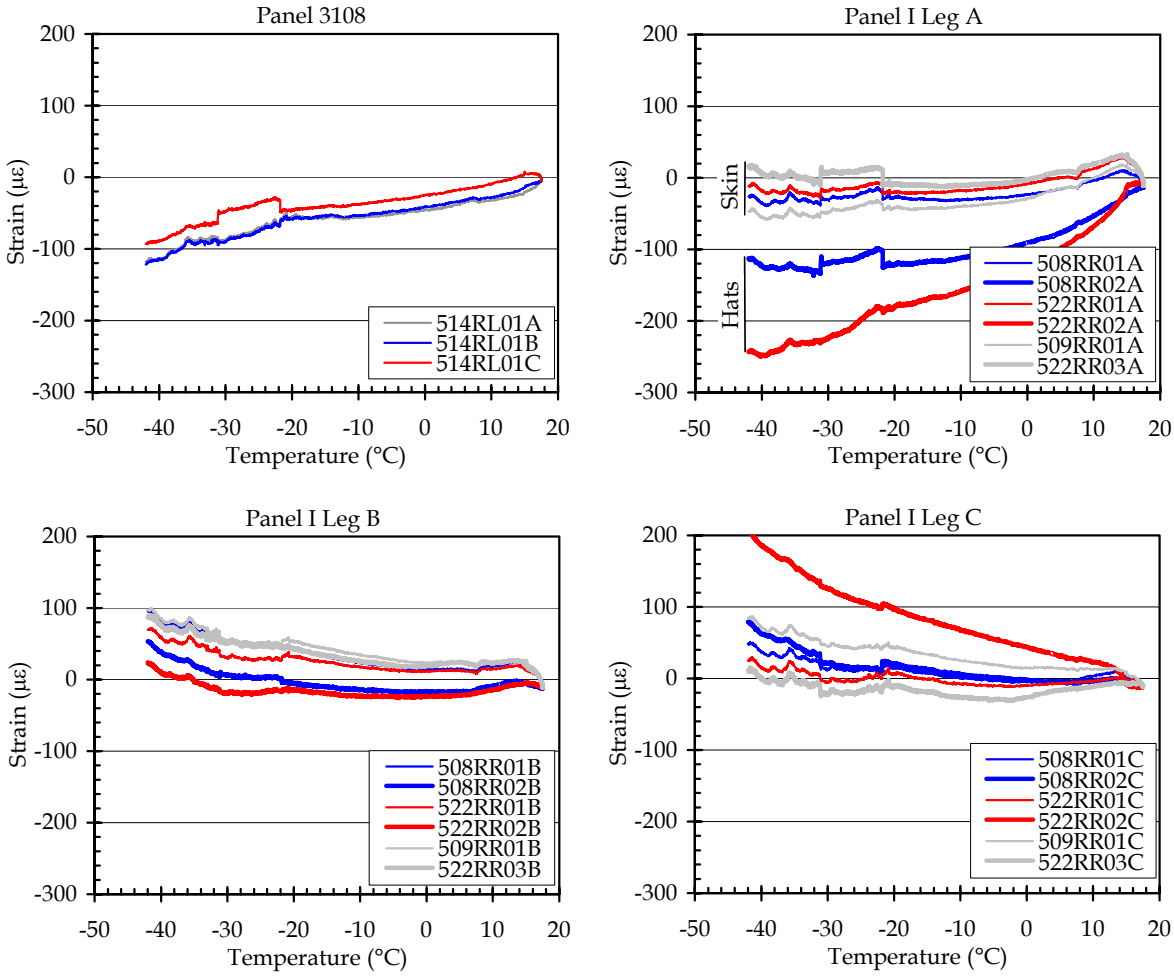

Figure 6: The effect of temperature on strains in Panels 3108 and I

These observations of the differences between Panel I and 3208 qualitatively matched the expected behaviour. The CTE of the aluminium (23.4 ppm °C^{-1}) and steel (11.2 ppm °C^{-1}) sub-structure was substantially higher than that of the composite Panel I (3.0 ppm °C^{-1}). The aircraft sub-structure was therefore expected to contract more that Panel I during cool-down, creating tensile strains in the sub-structure and compression strains on Panel I.

3.2.2.3 Summary

It appears that the difference in thermal strains resulting from the incorporation of a CRP into an aircraft are relatively modest, up to 200 με was observed in the CRPSS. If the 363.5 με fixed strain deviation band from reference [3] were used then it would be judged that the incorporation of Panel I had no effect on the thermally induced strains.

In the CRPSS this difference subtracted from the existing thermal strains and reduced the absolute magnitude of strain in the sub-structure. It is possible that incorporating components with reduced CTE into the sub-structure of a metallic aircraft, such as CRPs, actually reduces the strains in the local sub-structure. It certainly was the case for sub-ambient temperatures. However additional analysis and tests are required to validate this for elevated temperature.

Most of the thermal strains from the cool-down were less than 200 με. In reference [3], gauges where the peak strain was less than 200 με were categorised as "small strain error" gauges. Data from these gauges was ignored because the load transferred through such structure was not significant and so not of interest for validating the ILM. It was also argued that experimental errors could have large influences on these small strain results. In contrast to this approach the data from such gauges in the CRPSS were retained, primarily because eliminating them would have reduced substantially the already small data set. The consistent trends and magnitudes that were observed in the CRPSS data supported the retention.

In reference [1] the ILM was not used to predict the effects of the cool-down (sub-ambient temperature in the absence of applied mechanical load). This analysis has not been conducted and so the capability of the ILM to predict thermal strains only has not been validated. It is unlikely that this capability will be required in any future airworthiness application for the CRPT because predicting the effect of a temperature change only is not expected to be required. Predictions for airworthiness certification purposes would require the both temperature and airframe loading be considered.

3.3 Effect of mechanical loading

This section reports on the correlation between the strain data supplied in references [3] and [5] and the predictions made in references [1] and [3]. Demonstrating a satisfactory correlation between the ILM predictions from reference [1] and CRPSS strain gauge results would validate the design approach used for the demonstrator CRP.

In this Section strains are plotted as a function of the "consolidated CPLT load". This was referred to as the "consolidated load level" in Appendix A and is effectively a measure of the fraction of maximum load level for the particular load case.

Data channels were zeroed immediately prior to the commencement of each loadcase and recording continued until the loadcase was completed. No temperature compensation was applied to the strain data because the CRPSS was considered isothermal. The temperature during each of the CPLT loadcases varied by 0.2 °C or less, which would have corresponded to a difference of less than 4 με in the measured strains.

The strain versus consolidated load level for each of the CRPSS strain gauges are plotted in Figs 7 to 11. These figures also contain the ILM predicted strains from reference [1] (discussed in Section 3.4.4). The strain scale for most of the plots are different because of the wide range in the data. This does make comparison more difficult but does allow any features of the data to be observed more clearly.

Inspection of Figs 7 to 11 shows that strains were an approximately linear function of consolidated load level for most gauges except for some locations/loadcases on the FS 496 Former and Panel I. There was a distinct relaxation behaviour in the FS 496 former, FS 531 former and Panel I during the loading holds at 20, 40, 60 and 80 % consolidated load level. Finally, examination of the raw data showed that hysteresis during unloading was less than 50 με for most of the sub-structure. It was slightly larger than this on the FS 531 former and Panel I.

3.4 Comparisons

For each gauge and loadcase the strains defined in Equations 7 to 10 were calculated. These strains are reported in Tables 3 to 7, although only the Leg strains are discussed.

$$\varepsilon_{ac} = \varepsilon_b - \left(\frac{\varepsilon_a + \varepsilon_c}{2} \right) \tag{7}$$

$$\varepsilon_{max} = \left(\frac{\varepsilon_a + \varepsilon_c}{2} \right) + \sqrt{\left(\frac{\varepsilon_a - \varepsilon_c}{2} \right)^2 + \varepsilon_{ac}^{\,2}} \tag{8}$$

$$\varepsilon_{min} = \left(\frac{\varepsilon_a + \varepsilon_c}{2} \right) - \sqrt{\left(\frac{\varepsilon_a - \varepsilon_c}{2} \right)^2 + \varepsilon_{ac}^{\,2}} \tag{9}$$

$$\gamma_{xymax} = \varepsilon_{max} - \varepsilon_{min} \tag{10}$$

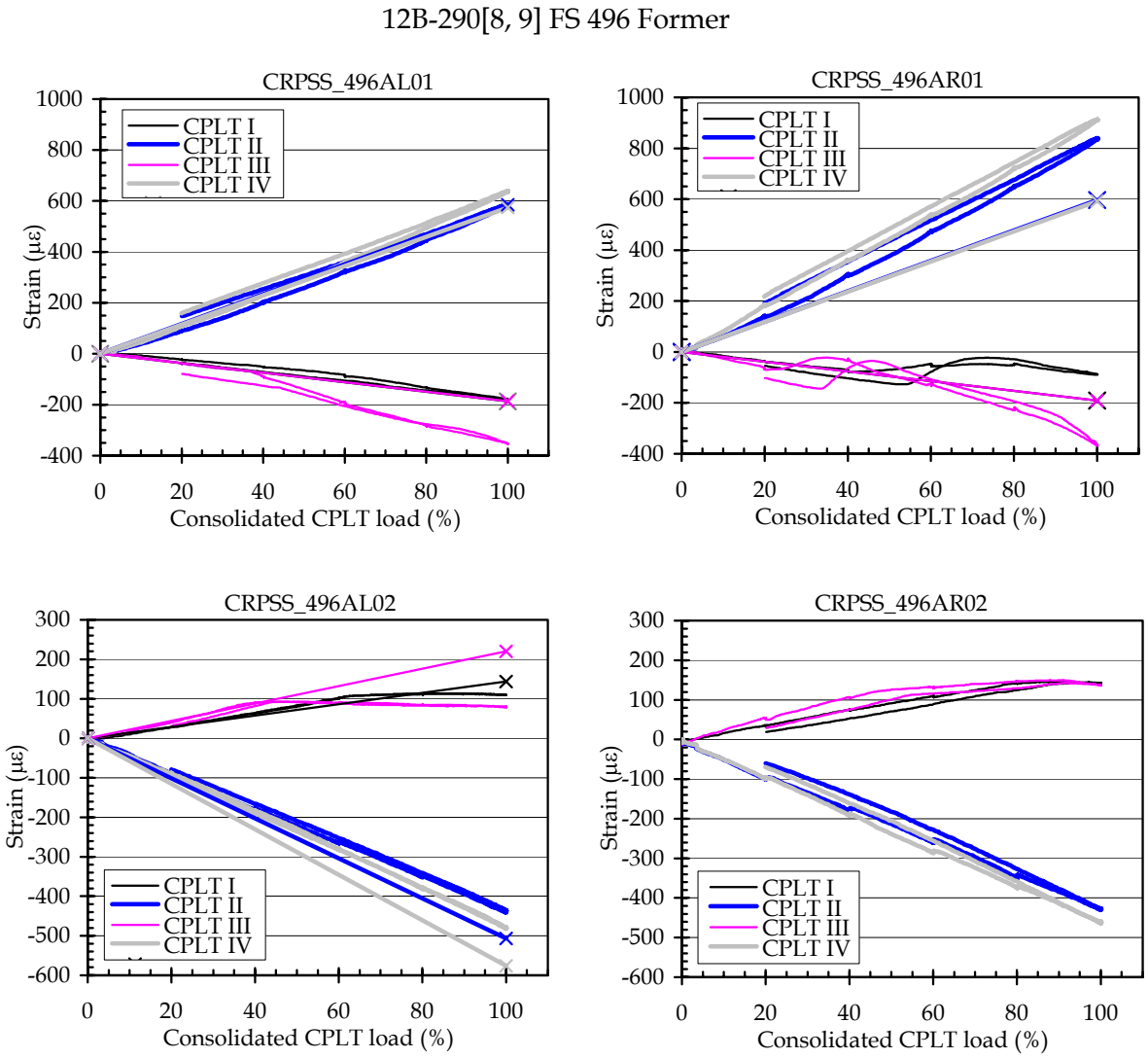

Figure 7: Measured (curves) and predicted (straight lines) CRPSS strains for the FS496 Former

where:

ε_{ac} = in-plane shear strain
ε_{max} = maximum principal strain
ε_{min} = minimum principal strain
γ_{xymax} = maximum in-plane shear strain
ε_a = strain in Leg A of the strain gauge
ε_b = strain in Leg B of the strain gauge
ε_c = strain in Leg C of the strain gauge

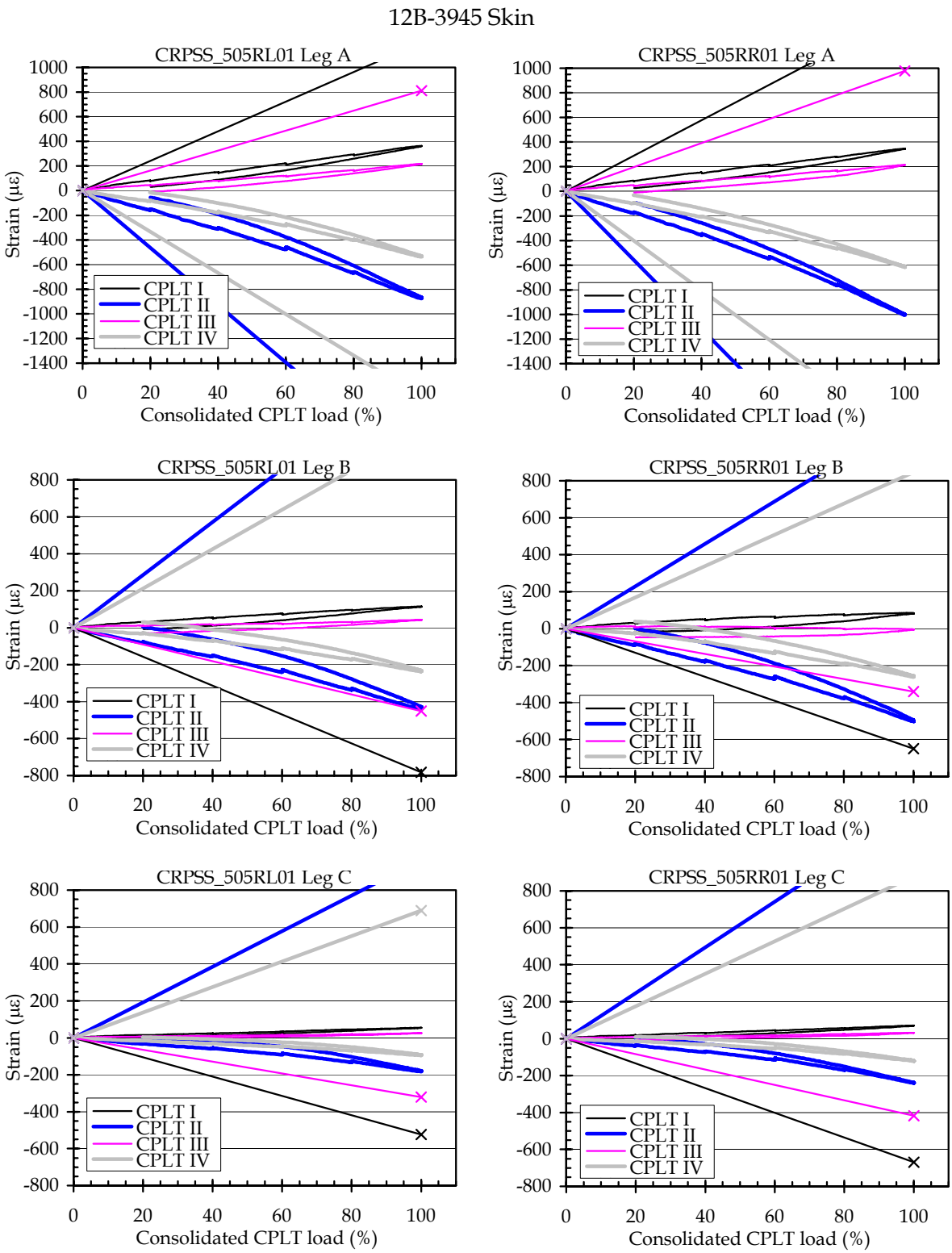

Figure 8: Measured (curves) and predicted (straight lines) CRPSS strains for the 12B-3945 Skin

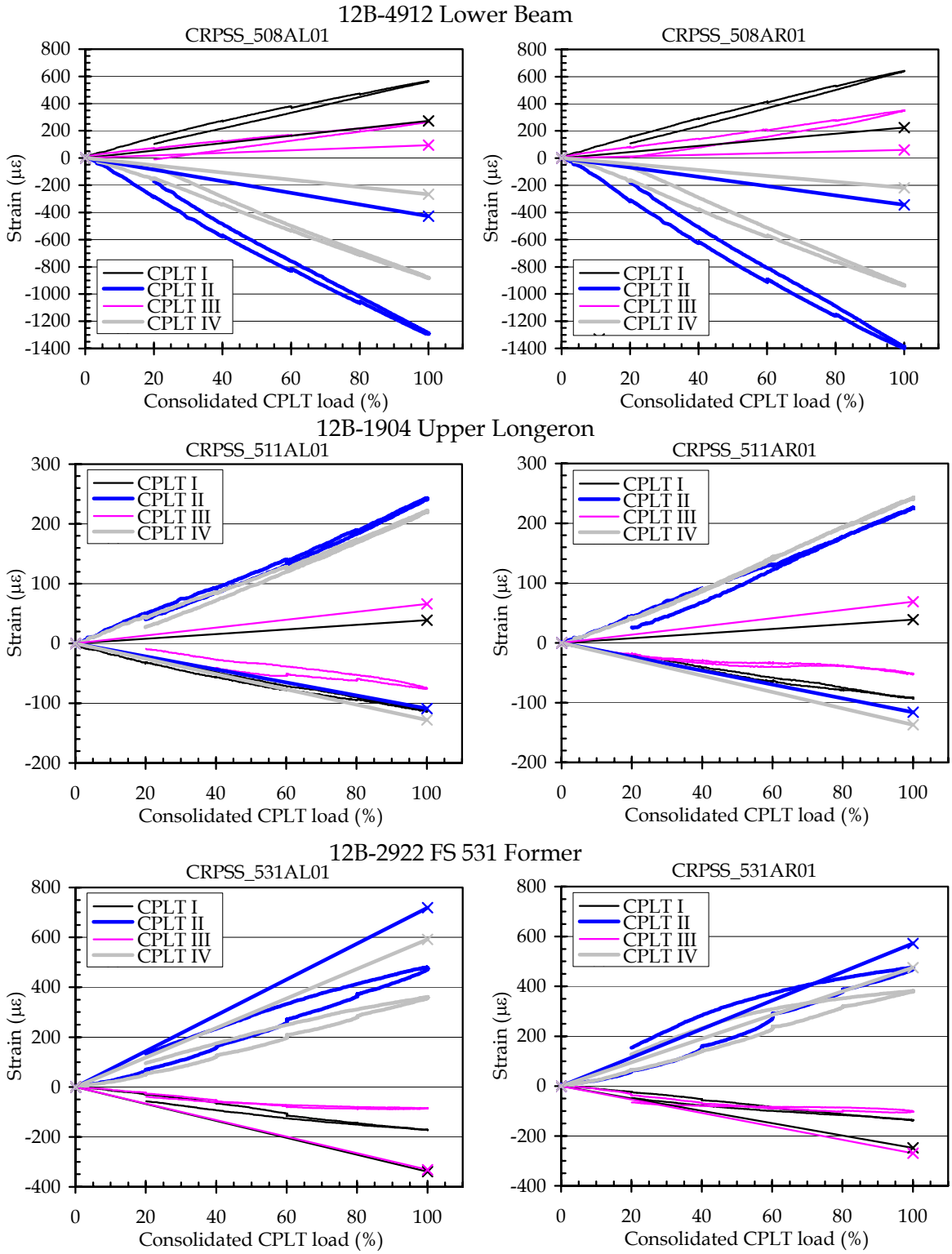

Figure 9: Measured (curves) and predicted (straight lines) CRPSS strains for the Lower Beam Upper Longeron and FS531 Former

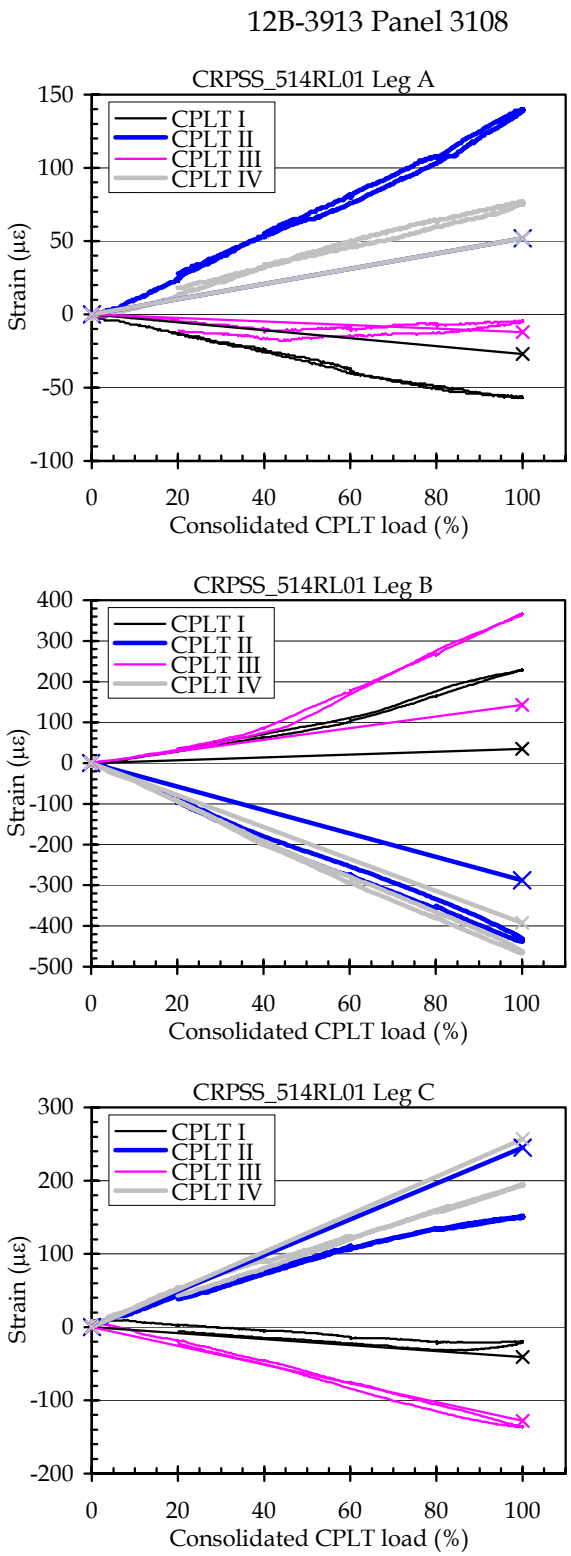

Figure 10: Measured (curves) and predicted (straight lines) CRPSS strains for Panel 3108

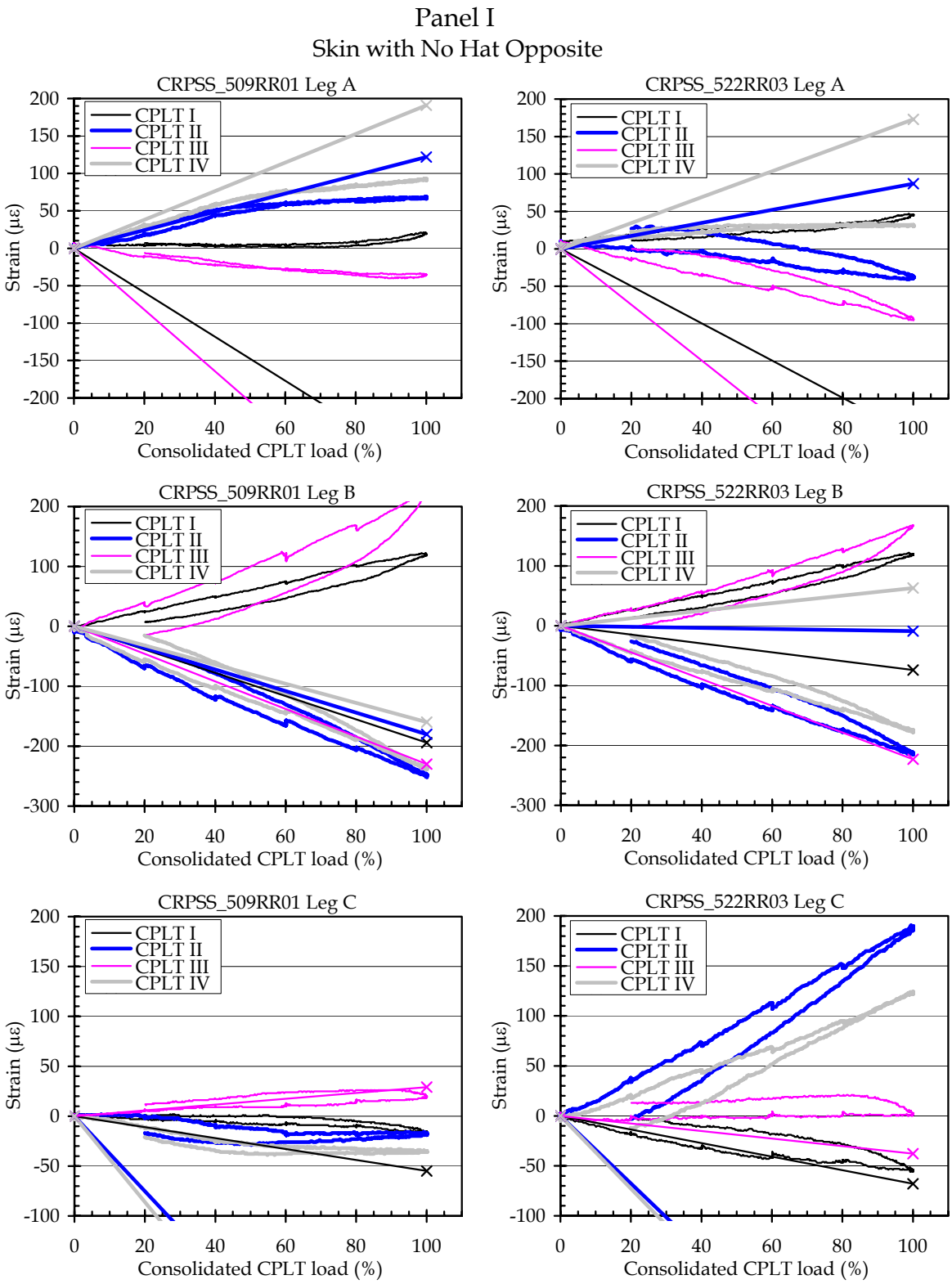

Figure 11: Measured (curves) and predicted (straight lines) CRPSS strains for Panel I …cont.

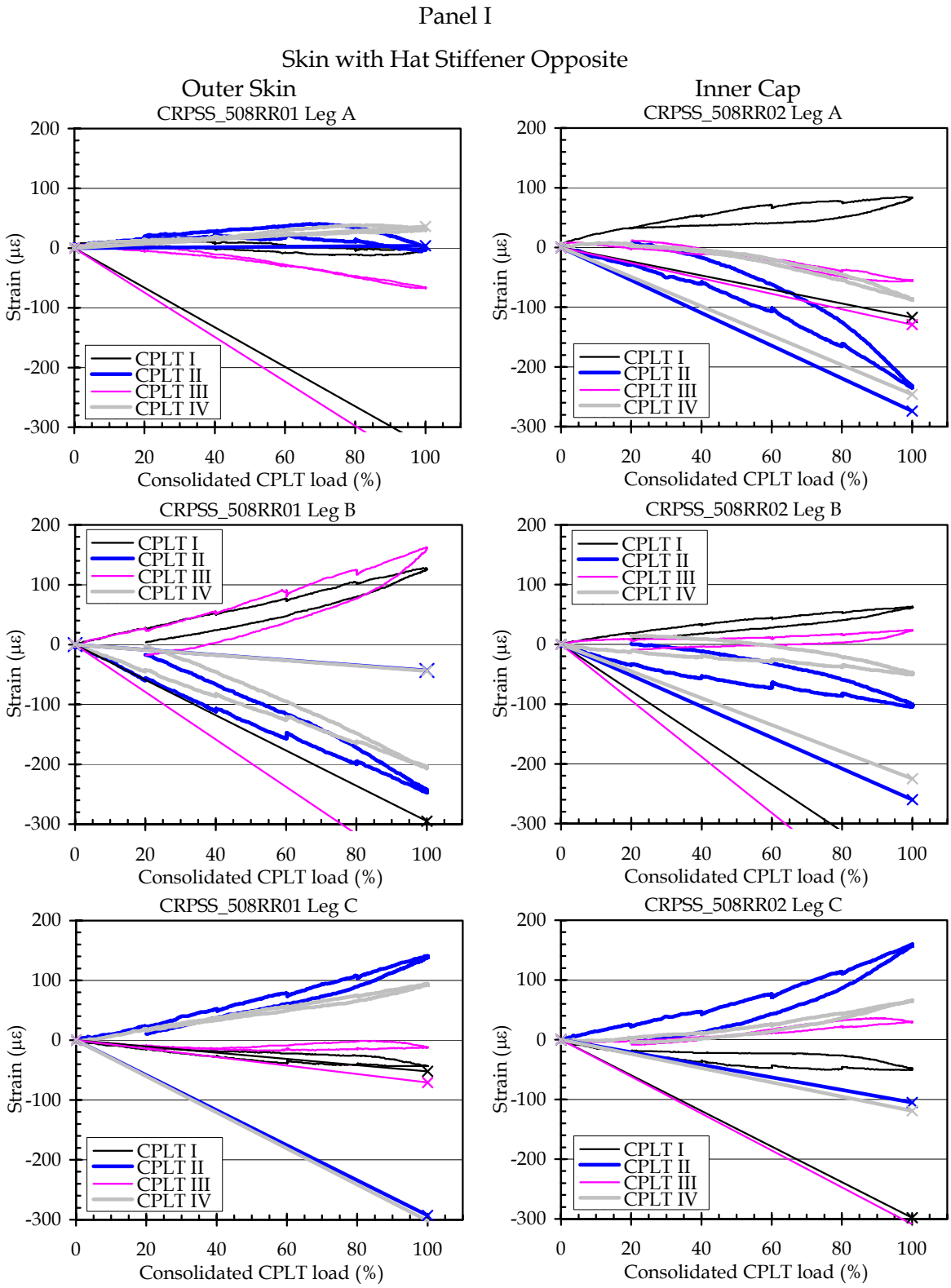

…cont. Figure 11: Measured (curves) and predicted (straight lines) CRPSS strains for Panel I

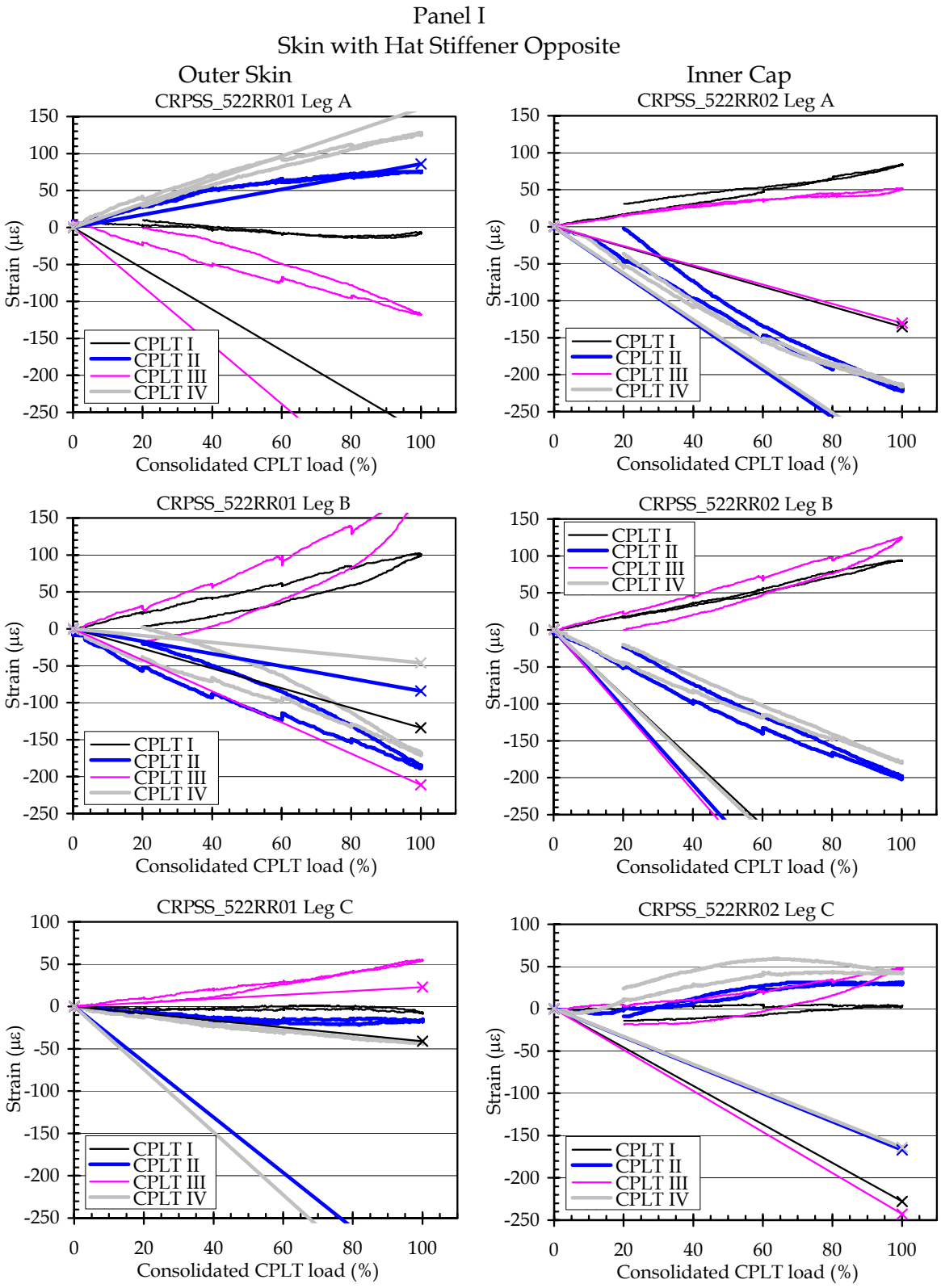

…cont. Figure 11: Measured (curves) and predicted (straight lines) CRPSS strains for Panel I

3.4.1 CRPSS left hand side compared to right hand side

Inspection of Figs 7-9 shows that the behaviour of gauges located on opposite sides of the aircraft was very similar. In almost all cases the direction (tension/compression) and ranking of strains for each CPLT loadcase was the same. For example the strains from CRPSS_496AL01 and CRPSS_496AR01 were, from maximum to minimum, CPLT IV, CPLT II, CPLT I then CPLT III.

The peak measured and calculated strains are shown in Table 3. These were very similar, with average differences of only 59 με between the Leg A gauges.

One set of strain gauge rosettes were located in equivalent positions on opposite sides of the aircraft, CRPSS_505RL01 and CRPSS_505RR01 on the 12B-3945 Skins. As with the uniaxial gauges, the measured strains from the gauges on the left and right sides were very close, as indicated in the final row of Table 3.

There were no gauges on Panel I that were directly comparable (opposite) to the rosette CRPSS_514RL01 located on Panel 3108. CRPSS_509RR01, a gauge on the outer skin of Panel I, was selected to provide a comparison of the strains in Panels 3108 and I. As shown in Figs 10 and 11, the response of the gauges on Panel I was quite different to those on Panel 3108. This is not surprising given that Panel 3108 was of aluminium honeycomb construction and Panel I was manufactured from advanced fibre composite materials and consisted of a thin skin with hat and z section stiffeners. Despite this difference in the

Table 3: Measured and predicted strains for left and right hand CRPSS gauges

Chann.	Gauge	Location	Loadcase	εa (με)			εb (με)			εc (με)			εac (με)			εmax (με)			εmin (με)			γxymax (με)		
				Left	Right	Δ	Left	Right	Δ	Left	Right	Δ	Left	Right	Δ	Left	Right	Δ	Left	Right	Δ	Left	Right	Δ
1-2	CRPSS_496AL01 CRPSS_496AR01	12B-290[8,9] FS496 Former	CPLT I	-180	-88	92																		
			CPLT II	585	838	253																		
			CPLT III	-354	-367	-13																		
			CPLT IV	638	913	276																		
3-4	CRPSS_496AL02 CRPSS_496AR02		CPLT I	110	143	33																		
			CPLT II	-438	-428	10																		
			CPLT III	79	137	58																		
			CPLT IV	-480	-462	19																		
5-10	CRPSS_505RL01 CRPSS_505RR01	12B-3945 Skin	CPLT I	362	345	-17	113	83	-30	54	69	15	-95	-124	-30	389	393	4	27	21	-6	362	372	10
			CPLT II	-870	-1001	-131	-430	-498	-68	-180	-239	-59	94	122	27	-167	-220	-53	-883	-1020	-137	716	801	85
			CPLT III	217	212	-4	42	-6	-48	25	32	7	-79	-128	-49	245	279	34	-3	-35	-32	248	313	66
			CPLT IV	-534	-612	-78	-234	-258	-24	-93	-120	-27	80	108	28	-79	-97	-18	-548	-634	-87	468	537	69
11-12	CRPSS_508AL01 CRPSS_508AR01	12B-4912 Lower Beam	CPLT I	564	641	77																		
			CPLT II	-1290	-1392	-102																		
			CPLT III	268	351	84																		
			CPLT IV	-881	-935	-55																		
13-14	CRPSS_511AL01 CRPSS_511AR01	12B-1904 Upper Long.	CPLT I	-112	-93	20																		
			CPLT II	242	226	-17																		
			CPLT III	-75	-51	24																		
			CPLT IV	221	242	21																		
15-17	CRPSS_514RL01 CRPSS_509RR01	12B-3913 Panel 3108	CPLT I	-57	20	76	229	119	-110	-20	-17	3	267	117	-150	229	120	-109	-306	-117	189	536	237	-298
			CPLT II	139	67	-72	-434	-248	187	151	-17	-168	-579	-273	306	724	301	-423	-434	-251	183	1158	552	-606
			CPLT III	-4	-36	-32	366	223	-143	-135	20	155	436	232	-204	371	225	-146	-510	-241	269	881	467	-415
			CPLT IV	77	93	16	-464	-236	228	194	-35	-229	-600	-265	335	738	302	-437	-467	-244	224	1206	545	-660
18-19	CRPSS_531AL01 CRPSS_531AR01	12B-2922 FS531 Former	CPLT I	-172	-137	35																		
			CPLT II	475	472	-3																		
			CPLT III	-85	-102	-17																		
			CPLT IV	358	380	23																		
Average of absolute value		All gauges				59			105			83			141			153			141			276
		12B-3945 only							43			27			34			27			65			57

strain/load behaviour, the measured and calculated strains were well within the fixed strain deviation band of ±363.5 με that was used in reference [3]. This result should be treated with caution because it is likely that it was the very low absolute strains in these panels that caused the differences to fall within this band.

Notwithstanding the previous paragraph, the similarity between left and right hand sides of the aircraft were expected. Panel I was designed to match the stiffness of Panel 3208 and the CRPSS was an isothermal test. Relative to Panel 3208, Panel I had a very similar axial stiffness but approximately twice the shear stiffness. It was not possible to match both the axial and shear stiffness of Panel I with that of Panel 3208. The number of 0/90° fabric plies in Panel I was dictated by the stiffness requirements. ±45 ° plies were then added to reduce strains to a level acceptable for fatigue considerations. These plies increased substantially the shear stiffness of Panel I. Clearly the high shear stiffness influenced, albeit moderately, load transfer in the local sub-structure.

3.4.2 CRPSS compared to FSS

Table 4 shows the data from the CRPSS and FSS in those locations that contained

Table 4: Measured and predicted strains for CRPSS and corresponding F-111C FSS gauges

Chann	Gauge	Location	Loadcase	εa (με)			εb (με)			εc (με)			εac (με)			εmax (με)			εmin (με)			γxymax (με)		
				CRPSS	FSS	Δ	CRPSS	FSS	Δ	CRPSS	FSS	Δ	CRPSS	FSS	Δ	CRPSS	FSS	Δ	CRPSS	FSS	Δ	CRPSS	FSS	Δ
1-2	CRPSS_496AL01 C496AL38	12B-290[8,9] FS496 Former	CPLT I	-180	-203	-23																		
			CPLT II	585	744	159																		
			CPLT III	-354	-468	-114																		
			CPLT IV	638	771	133																		
3-4	CRPSS_496AL02 C496AL35		CPLT I	110	141	31																		
			CPLT II	-438	-393	45																		
			CPLT III	79	76	-3																		
			CPLT IV	-480	-422	58																		
5-10	CRPSS_505RL01 C505RL01	12B-3945 Skin	CPLT I	362	455	93	113	154	41	54	-84	-138	-95	-32	63	389	457	68	27	-86	-113	362	543	181
			CPLT II	-870	-1566	-696	-430	-321	109	-180	279	459	94	323	228	-167	334	501	-883	-1621	-738	716	1954	1238
			CPLT III	217	253	36	42	117	75	25	-58	-83	-79	20	98	245	254	9	-3	-59	-56	248	313	65
			CPLT IV	-534	-1066	-532	-234	-259	-25	-93	182	275	80	183	103	-79	208	287	-548	-1092	-545	468	1300	832
11	CRPSS_508AL01 C508AL02	12B-4912 Lower Beam	CPLT I	564	584	20																		
			CPLT II	-1290	-1138	152																		
			CPLT III	268	277	9																		
			CPLT IV	-881	-795	86																		
12	CRPSS_508AR01 C508AR02		CPLT I	641	571	-70																		
			CPLT II	-1392	-1276	116																		
			CPLT III	351	293	-58																		
			CPLT IV	-935	-933	2																		
13	CRPSS_511AL01 C510AL03	12B-1904 Upper Long.	CPLT I	-112	-137	-25																		
			CPLT II	242	289	47																		
			CPLT III	-75	-112	-37																		
			CPLT IV	221	290	69																		
14	CRPSS_511AR01 C510AR03		CPLT I	-93	-109	-16																		
			CPLT II	226	245	19																		
			CPLT III	-51	-100	-49																		
			CPLT IV	242	258	16																		
15-17	CRPSS_514RL01 C514RL01	12B-3913 Panel 3108	CPLT I	-57	-60	-3	229	163	-66	-20	-33	-13	267	210	-58	229	164	-66	-306	-257	49	536	420	-115
			CPLT II	139	112	-27	-434	-374	60	151	176	25	-579	-518	61	724	662	-62	-434	-375	59	1158	1037	-121
			CPLT III	-4	-20	-16	366	288	-78	-135	-119	16	436	358	-78	371	292	-79	-510	-430	81	881	721	-160
			CPLT IV	77	54	-23	-464	-391	73	194	193	-1	-600	-515	85	738	643	-96	-467	-395	72	1206	1038	-168
18	CRPSS_531AL01 C531AL05	12B-2922 FS531 Former	CPLT I	-172	-152	20																		
			CPLT II	475	273	-202																		
			CPLT III	-85	-70	15																		
			CPLT IV	358	179	-179																		
Average of absolute value		All gauges				89			66			126			97			146			214			360
		w/o 505RL01, II & IV				58			66			46			74			63			72			135

gauges during both tests. There was a good match between the two tests, with average differences of 89 με for Leg A gauges. A significant component of this difference was induced by gauges on the left hand 12B-3945 Skin (CRPSS_505RL01) during CPLT II and IV. Ignoring these outliers reduced the average difference in the legs to approximately 60 με. Again, both of these were well within the ±363.5 με fixed strain deviation band used in reference [3].

Overall there were no significant differences in the strains measured during the CRPSS and FSS. This supports the use of the ILM that was correlated for A8-144, in the analysis of the CRPSS.

3.4.3 F-111C FSS compared to ILM prediction from reference [3]

The measured and predicted strains for the FSS, as shown in reference [3], are compared in Table 5. This was done to establish a baseline against which the data for the CRPSS could be compared.

Table 5: Measured and predicted strains for the FSS

Chann	Gauge	Location	Loadcase	εa (με)			εb (με)			εc (με)			εac (με)			εmax (με)			εmin (με)			γxymax (με)		
				FSS	Pred.	Δ	FSS	Pred.	Δ	FSS	Pred.	Δ	FSS	Pred.	Δ	FSS	Pred.	Δ	FSS	Pred.	Δ	FSS	Pred.	Δ
1-2	C496AL38	12B-290[8,9] FS496 Former	CPLT I	-203	-259	-56																		
			CPLT II	744	588	-156																		
			CPLT III	-468	-289	179																		
			CPLT IV	771	597	-174																		
3-4	C496AL35		CPLT I	141	221	80																		
			CPLT II	-393	-538	-145																		
			CPLT III	76	328	252																		
			CPLT IV	-422	-631	-209																		
5-10	C505RL01	12B-3945 Skin	CPLT I	455	1145	690	154	-761	-915	-84	-491	-407	-32	-1088	-1057	457	1688	1232	-86	-1034	-948	543	2722	2179
			CPLT II	-1566	-2374	-808	-321	1471	1792	279	970	691	323	2173	1851	334	2040	1706	-1621	-3444	-1824	1954	5484	3530
			CPLT III	253	756	503	117	-456	-573	-58	-294	-236	20	-687	-707	254	1095	841	-59	-633	-575	313	1728	1415
			CPLT IV	-1066	-1665	-599	-259	1080	1339	182	674	492	183	1576	1393	208	1467	1259	-1092	-2457	-1365	1300	3924	2624
11	C508AL02	12B-4912 Lower Beam	CPLT I	584	219	-365																		
			CPLT II	-1138	-379	759																		
			CPLT III	277	54	-223																		
			CPLT IV	-795	-214	581																		
12	C508AR02		CPLT I	571	240	-331																		
			CPLT II	-1276	-422	854																		
			CPLT III	293	69	-224																		
			CPLT IV	-933	-247	686																		
13	C510AL03	12B-1904 Upper Long.	CPLT I	-137	44	181																		
			CPLT II	289	-117	-406																		
			CPLT III	-112	72	184																		
			CPLT IV	290	-138	-428																		
14	C510AR03		CPLT I	-109	45	154																		
			CPLT II	245	-118	-363																		
			CPLT III	-100	73	173																		
			CPLT IV	258	-140	-398																		
15-17	C514RL01	12B-3913 Panel 3108	CPLT I	-60	-34	26	163	106	-57	-33	-53	-20	210	150	-60	164	106	-57	-257	-194	63	420	300	-120
			CPLT II	112	69	-43	-374	-325	49	176	189	13	-518	-454	64	662	587	-75	-375	-329	45	1037	917	-121
			CPLT III	-20	-32	-12	288	256	-32	-119	-129	-10	358	337	-21	292	259	-32	-430	-420	10	721	679	-42
			CPLT IV	54	72	18	-391	-458	-67	193	211	18	-515	-600	-85	643	744	102	-395	-462	-67	1038	1206	168
18	C531AL05	12B-2922 FS531 Former	CPLT I	-152	-46	106																		
			CPLT II	273	104	-169																		
			CPLT III	-70	-53	17																		
			CPLT IV	179	98	-81																		
Ave of absolute value		All gauges				295			603			236			655			663			612			1275

Table 5 shows that the trends and ranking of predicted strains generally matched those of the measured strains. For example in C496AL38 the ranking of both measured (FSS) and predicted (Pred.) strain, from minimum to maximum, was CPLT II, CPLT I, CPLT III and CPLT IV. Exceptions to this pattern were observed on the Upper Longeron (12B-1904) and 12B-3945 Skin, Legs B and C. In these cases the predicted strains were opposite in sign to the measured strains. For example C510AL03 the measured strains for CPLT I, II, III and IV were –137, 289, -112 and 290 respectively. The predicted strains for the corresponding loadcases were 44, -117, 72 and –138. Clearly the ILM did not predict the behaviour of the structure in these regions. This behaviour was not detected or discussed in reference [3] because a detailed outlier analysis was not conducted for the nacelle assembly.

The measured and predicted strains from the FSS are plotted in Figure 12. Approximately half of the data from this test was outside the ±363.5 με fixed strain deviation band. Deviations of this magnitude were observed in reference [3] and judged as acceptable.

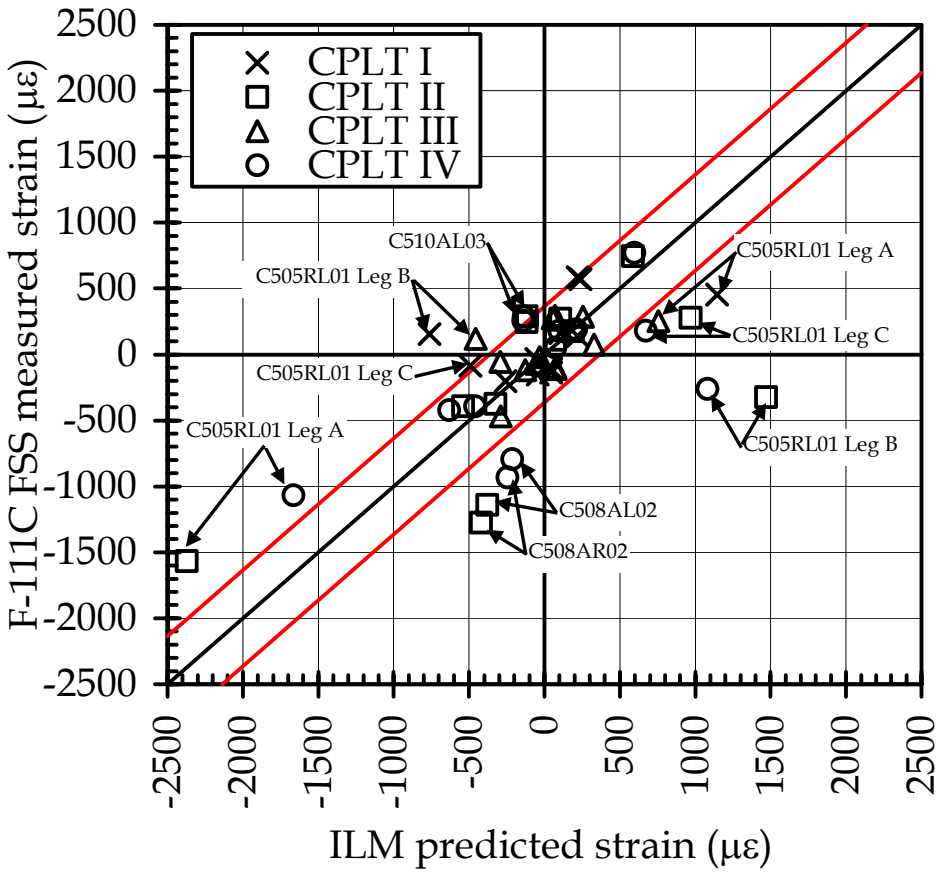

Figure 12: Measured and predicted strains from the FSS. The central diagonal line indicates a perfect match while the outer diagonals show the ±363.5 με fixed deviation band

The majority of the outliers in Figure 12 were caused by the C505 strain gauges on the 12B-3945 Skin. The axial strains on this part were over-predicted for CPLT II (+7.33 g @ 56° wing sweep) and IV (+7.33 g @ 26° wing sweep) and under predicted during CPLT I (-2.40 g @ 56° sweep) and III (-3.00 g @ 26° wing sweep). The positive g loading in CPLT II and IV bent the aircraft wings up and loaded the lower fuselage including 12B-3945 Skin in axial compression. CPLT I and III bent the wings down and loaded the Skin in axial tension. In both cases the magnitude of the measured strain was less than that predicted. It is most likely that all of these differences were a result of the technique used to model the joint between the sub-structure and the panel. An overlapping element method was used in the ILM because this reduced model complexity, however it produced very stiff joints. Skin panels on real aircraft are connected by single rows of fasteners bearing on imperfect countersunk holes with a gap between the panel and nut-plate. This situation is much more compliant than the modelled joint.

Finally, the C508 gauges on the 12B-4912 Lower Beam were under-predicted during CPLT II and IV. There is no apparent reason for this difference.

3.4.4 CRPSS compared to ILM predictions from reference [1]

Tables 6 and 7 show, respectively, the strains measured by the CRPSS sub-structure and Panel I gauges compared to those predicted by the ILM used in reference [1].

Five Nastran job runs were used for these predictions. The first four were of the full ILM (F-111C_CPLT[I, II, III, V]_pat_equiv_therm from reference [1]) while the last run was made with the sub-model (ilm-comp-therm.db from reference [1]). The full ILM runs were used to obtain the boundary translations and rotations for the fine grid sub-model. These runs contained predictions for the strain gauges on the sub-structure. The sub-model runs were used to predict the behaviour of Panel I.

Predictions were not extracted for CRPSS_496AR02 because these results were not calculated in the FE runs. The gauge was located at the transition between the ILM and Panel I and was located on the Z2 surface of the elements at the gauge location. The analysis runs where strains for the Z2 surfaces were calculated were done using the F-111C_CPLT[I, II, III, V]_pat_equiv_therm models. These models did not contain elements at the position of CRPSS_496AR02. The ilm-comp-therm.db sub-model run did contain elements corresponding to the location of the gauge, however the Z2 strains were not calculated in this run. Given that results exist for all the other gauges, it was decided not to proceed with reworking the models to obtain the prediction for CRPSS_496AR02.

The measured and predicted strains from Table 6 were plotted in Figure 13. As with Figure 12, much of the data fell within the ±363.5 με fixed strain deviation band. However approximately twice the number of the predictions for CRPSS gauges fell outside the band than for the FSS gauges.

Table 6: Measured and predicted sub-structure strains for the CRPSS

Chann	Gauge	Location	Loadcase	εa (με)			εb (με)			εc (με)			εac (με)			εmax (με)			εmin (με)			γxymax (με)		
				CRPSS	Pred.	Δ	CRPSS	Pred.	Δ	CRPSS	Pred.	Δ	CRPSS	Pred.	Δ	CRPSS	Pred.	Δ	CRPSS	Pred.	Δ	CRPSS	Pred.	Δ
1	CRPSS_496AL01	12B-290[8,9] FS496 Former	CPLT I	-180	-187	-7																		
			CPLT II	585	585	0																		
			CPLT III	-354	-186	168																		
			CPLT IV	638	574	-64																		
2	CRPSS_496AR01		CPLT I	-88	-191	-103																		
			CPLT II	838	597	-241																		
			CPLT III	-367	-191	176																		
			CPLT IV	913	593	-320																		
3	CRPSS_496AL02		CPLT I	110	144	34																		
			CPLT II	-438	-507	-68																		
			CPLT III	79	220	141																		
			CPLT IV	-480	-576	-95																		
4	CRPSS_496AR02		CPLT I	143																				
			CPLT II	-428																				
			CPLT III	137																				
			CPLT IV	-462																				
5-7	CRPSS_505RL01	12B-3945 Skin	CPLT I	362	1203	841	113	-783	-896	54	-524	-578	-95	-1122	-1027	389	1755	1366	27	-1077	-1104	362	2832	2470
			CPLT II	-870	-2326	-1456	-430	1431	1861	-180	963	1143	94	2113	2018	-167	1995	2162	-883	-3359	-2476	716	5354	4638
			CPLT III	217	812	595	42	-451	-493	25	-321	-346	-79	-697	-618	245	1144	899	-3	-652	-649	248	1796	1548
			CPLT IV	-534	-1672	-1138	-234	1065	1299	-93	689	782	80	1557	1477	-79	1462	1541	-548	-2445	-1897	468	3906	3438
8-10	CRPSS_505RR01		CPLT I	345	1440	1095	83	-649	-731	69	-669	-738	-124	-1034	-910	393	1862	1469	21	-1091	-1112	372	2954	2582
			CPLT II	-1001	-2797	-1796	-498	1146	1644	-239	1236	1475	122	1927	1805	-220	2008	2228	-1020	-3569	-2549	801	5578	4777
			CPLT III	212	978	766	-6	-340	-334	32	-418	-450	-128	-620	-492	279	1214	935	-35	-654	-619	313	1868	1555
			CPLT IV	-612	-2011	-1399	-258	846	1103	-120	878	998	108	1412	1304	-97	1453	1550	-634	-2587	-1953	537	4040	3503
11	CRPSS_508AL01	12B-4912 Lower Beam	CPLT I	564	273	-291																		
			CPLT II	-1290	-428	862																		
			CPLT III	268	95	-173																		
			CPLT IV	-881	-267	613																		
12	CRPSS_508AR01		CPLT I	641	224	-417																		
			CPLT II	-1392	-344	1048																		
			CPLT III	351	60	-291																		
			CPLT IV	-935	-218	717																		
13	CRPSS_511AL01	12B-1904 Upper Long.	CPLT I	-112	39	151																		
			CPLT II	242	-109	-351																		
			CPLT III	-75	66	141																		
			CPLT IV	221	-128	-349																		
14	CRPSS_511AR01		CPLT I	-93	39	131																		
			CPLT II	226	-116	-342																		
			CPLT III	-51	69	120																		
			CPLT IV	242	-137	-379																		
15-17	CRPSS_514RL01	12B-3913 Panel 3108	CPLT I	-57	-27	30	229	35	-194	-20	-41	-21	267	69	-198	229	34	-195	-306	-103	203	536	138	-398
			CPLT II	139	52	-87	-434	-288	146	151	245	94	-579	-437	143	724	596	-128	-434	-298	136	1158	894	-264
			CPLT III	-4	-12	-8	366	143	-223	-135	-128	7	436	213	-223	371	150	-221	-510	-291	219	881	440	-441
			CPLT IV	77	52	-25	-464	-392	73	194	257	63	-600	-546	54	738	710	-28	-467	-400	67	1206	1110	-96
18	CRPSS_531AL01	12B-2922 FS531 Former	CPLT I	-172	-339	-167																		
			CPLT II	475	719	244																		
			CPLT III	-85	-332	-247																		
			CPLT IV	358	592	234																		
19	CRPSS_531AR01		CPLT I	-137	-248	-111																		
			CPLT II	472	572	100																		
			CPLT III	-102	-269	-167																		
			CPLT IV	380	475	95																		

In the sub-structure, almost every outlier was located in either the CRPSS_505 gauges on the 12B-3945 Skin or the CRPSS_508 gauges on the 12B-4912 Lower Beam. The over- and under-predictions were in the same sense as with the FSS, suggesting that both models behaved similarly. The errors in predictions did not appear to be related to the side of the aircraft, left or right, suggesting that the inclusion of Panel I did not influence greatly the strains within the 12B-3945 Skin.

Table 7: Measured and predicted Panel I strains for the CRPSS

Chann	Gauge	Location	Loadcase	εa (με)			εb (με)			εc (με)			εac (με)			εmax (με)			εmin (με)			γxymax (με)		
				CRPSS	Pred.	Δ	CRPSS	Pred.	Δ	CRPSS	Pred.	Δ	CRPSS	Pred.	Δ	CRPSS	Pred.	Δ	CRPSS	Pred.	Δ	CRPSS	Pred.	Δ
20-22	CRPSS_508RR01	Panel I	CPLT I	-4	-331	-327	126	-295	-421	-43	-52	-9	150	-104	-253	128	-18	-146	-175	-365	-190	302	348	46
			CPLT II	-1	4	5	-245	-43	202	139	-293	-432	-314	102	416	390	35	-355	-252	-325	-73	643	360	-283
			CPLT III	-67	-372	-305	161	-396	-557	-12	-71	-59	201	-175	-375	163	9	-154	-242	-452	-210	405	460	55
			CPLT IV	32	36	4	-204	-44	161	94	-302	-396	-267	90	356	331	59	-272	-206	-325	-119	537	384	-153
23-25	CRPSS_508RR02		CPLT I	84	-117	-201	62	-391	-453	-49	-298	-249	45	-183	-228	98	-3	-101	-63	-412	-349	161	408	247
			CPLT II	-234	-274	-40	-102	-260	-158	159	-105	-264	-64	-71	-6	169	-79	-248	-244	-300	-56	413	220	-193
			CPLT III	-57	-129	-72	24	-470	-493	30	-309	-339	37	-251	-288	44	47	3	-70	-485	-415	114	532	418
			CPLT IV	-87	-246	-159	-49	-225	-176	65	-119	-184	-38	-43	-4	74	-106	-180	-96	-258	-162	171	152	-19
26-28	CRPSS_509RR01		CPLT I	20	-295	-315	119	-194	-312	-17	-55	-38	117	-19	-136	120	-54	-174	-117	-296	-179	237	242	5
			CPLT II	67	122	55	-248	-180	68	-17	-376	-359	-273	-53	220	301	127	-174	-251	-382	-131	552	510	-42
			CPLT III	-36	-410	-374	223	-230	-453	20	29	9	232	-40	-271	225	32	-193	-241	-414	-173	467	446	-21
			CPLT IV	93	191	98	-236	-160	77	-35	-430	-395	-265	-40	225	302	194	-108	-244	-432	-188	545	626	81
29-31	CRPSS_522RR01		CPLT I	-7	-277	-270	99	-134	-233	-8	-41	-33	107	26	-81	99	-39	-138	-114	-280	-166	213	242	29
			CPLT II	75	86	11	-187	-84	103	-16	-327	-311	-216	37	253	250	90	-160	-191	-330	-139	441	420	-21
			CPLT III	-118	-398	-280	186	-211	-397	54	23	-31	218	-24	-241	203	24	-179	-266	-399	-133	469	424	-45
			CPLT IV	127	161	34	-168	-46	123	-43	-371	-328	-211	60	270	269	167	-102	-185	-378	-193	454	546	92
32-34	CRPSS_522RR02		CPLT I	84	-135	-219	94	-440	-533	3	-228	-231	50	-258	-308	108	82	-26	-21	-444	-423	129	524	395
			CPLT II	-220	-322	-102	-199	-523	-323	30	-167	-197	-104	-278	-174	68	44	-24	-258	-533	-275	326	576	250
			CPLT III	52	-130	-182	124	-543	-667	49	-243	-292	74	-357	-431	124	174	50	-24	-548	-524	148	722	574
			CPLT IV	-215	-314	-99	-179	-451	-272	43	-164	-207	-93	-212	-119	73	-5	-78	-245	-472	-227	318	468	150
35-37	CRPSS_522RR03		CPLT I	46	-249	-295	119	-74	-193	-56	-68	-12	124	85	-39	129	-35	-164	-139	-282	-143	267	248	-19
			CPLT II	-38	87	125	-213	-9	203	187	-338	-525	-287	116	403	383	116	-267	-234	-367	-133	617	484	-133
			CPLT III	-95	-373	-278	167	-223	-389	1	-38	-39	214	-17	-231	172	-37	-209	-266	-374	-108	438	336	-102
			CPLT IV	32	173	141	-176	63	239	124	-364	-488	-254	159	412	336	216	-120	-180	-407	-227	516	624	108
Average of absolute value		All gauges				315			450			337			445			454			498			811
		Panel I				166			300			226			239			151			206			145

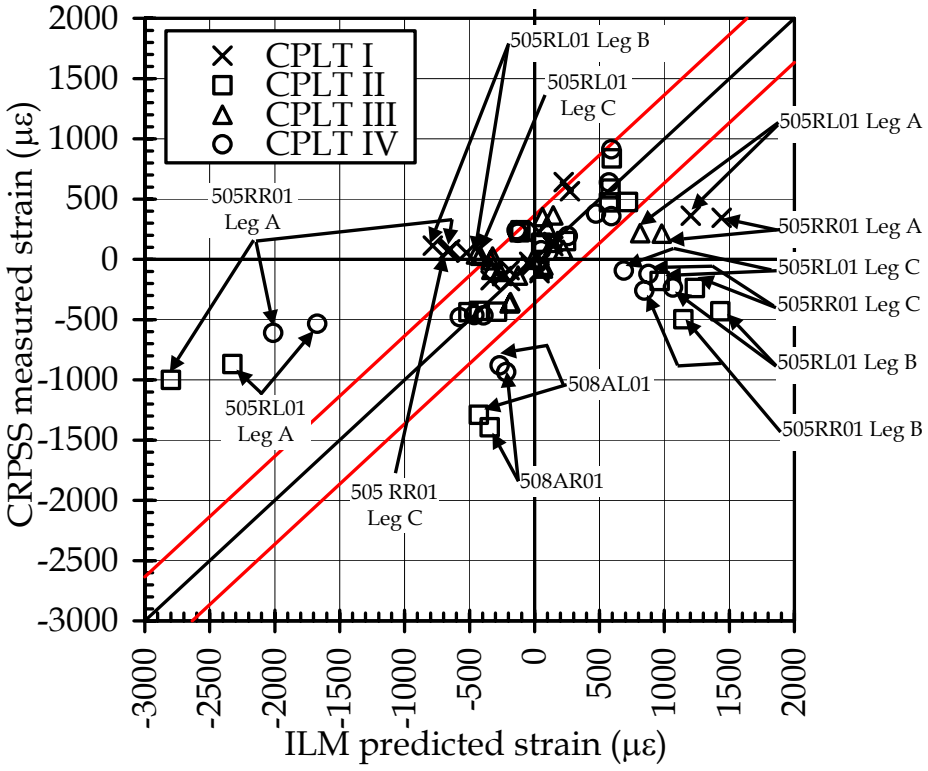

Figure 13: Measured and predicted sub-structure strains from the CRPSS. The central diagonal indicates a perfect match and the outer diagonals show the ±363.5 με fixed deviation band

As implied in Section 3.4.3 softening the modelled joint between the 12B-3945 Skin and sub-structure joint is expected to decrease the difference between measured and predicted strains. This was recognised prior to the initial predictions being made and, as reported in reference [1], the sub-models were created with a single row of equivalenced nodes at the fastener locations. While this approach may have softened the joints relative to the ILM, it appears that this alone was not sufficient to predict accurately the strains within the Skin. A further improvement would be to replace the equivalenced nodes with spring elements, the stiffness of which could be determined experimentally (using specimens that realistically simulate the actual joint, not just the fasteners perfectly bedded into perfect countersink holes) or by correlating the model predictions with the FSS and CRPSS strain data. Performing either of these approaches was beyond the scope of the program described in this report.

The ILM used for the CRPSS predictions was that valid in December 2002 while the version for the FSS was valid in October 2004. It is possible that the differences between Figs 12 and 13 may be reduced if the CRPSS predictions were re-run using the most recent version of the ILM. However, as stated above, it is likely that further modification of the sub-models would still be required to address the excessively stiff panel-to-skin joints. It would be logical to make both of these changes at the same time in any future rework of this analysis.

A possible further modification would be to refine the mesh throughout the entire sub-model. The ILM has a coarse grid mesh that is suitable for establishing the main load paths through the aircraft structure. When detailed stress and strain predictions are required it is usual to create a fine grid sub-model of the region and use the ILM to establish the boundary conditions for that fine grid sub-model. This was done to a limited extent in reference [1], the sub-model was made by inserting a fine-grid model of Panel I into the coarse grid sub-structure using a narrow transition region. In contrast, all strains measured during the FSS were compared directly with the predictions from the coarse grid ILM.

The measured and predicted strains from Table 7 were plotted in Figure 14. The ten channels where the predicted strain deviated by more than 364 με from the measured strain are labelled. The outliers contained at least one leg from each of the gauges on Panel I with all except one being from Leg's B and C. Measurements from the axial gauges were mostly within 300 με of predicted.

The magnitude of the measured strain tended to be less than that of the predicted strain. This was similar to that for the 12B-3945 Skin, so it appears that the reason for the over-predicted strains were excessively stiff joints between the Panel and sub- structure. The lack of Leg A gauges in the outliers suggest that the axial component was predicted better than the transverse and shear loads for this panel. This is consistent with the observation that a significant number of the holes in Panel I were elongated in the transverse direction (vertical direction, perpendicular to aircraft longitudinal axis) during installation so that

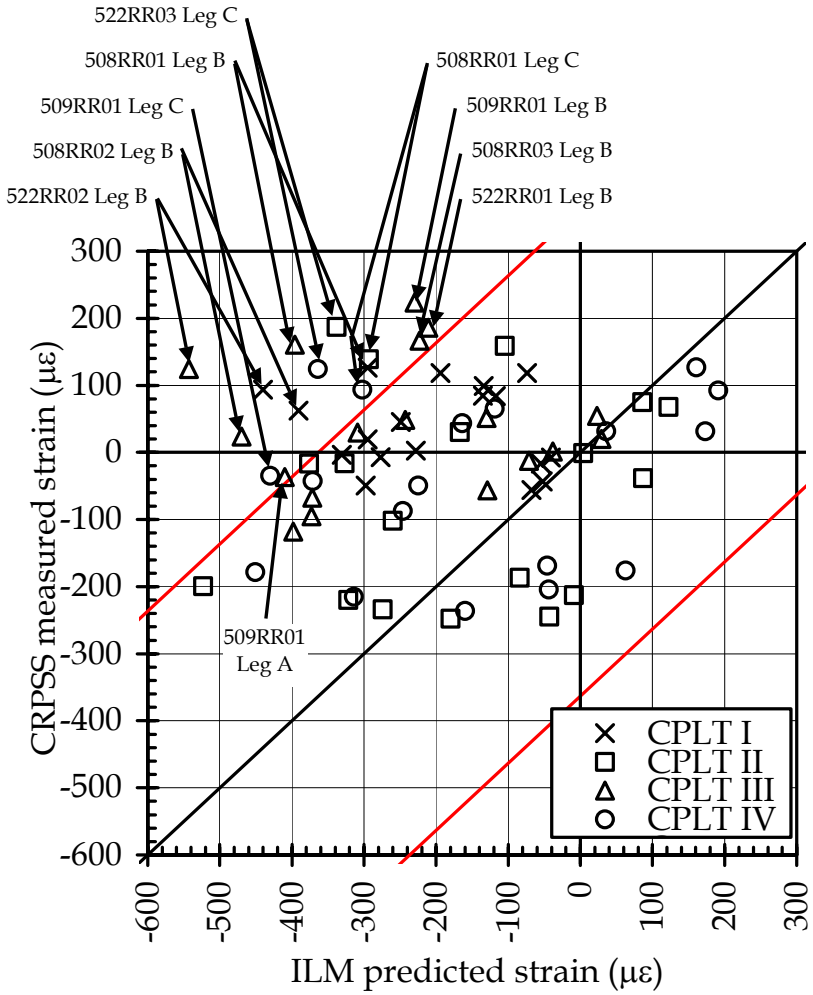

Figure 14: Measured and predicted panel I strains from the CRPSS. The central diagonal indicates a perfect match and the outer diagonals show the ±363.5 με fixed deviation band

the panel would fit the aircraft. Such rework would still be effective in restraining relative movement between the panel and sub-structure in the axial direction (aircraft longitudinal axis) but would be less effective for transverse and shear loads. Further work is required to verify that hole elongation could explain the observed strain differences.

4. Conclusions

The Composite Replacement Panel Strain Survey (CRPSS) was conducted in June 2004. In this test, a demonstrator Composite Replacement Panel (denoted Panel I) was installed on an F-111C aircraft prior to the aircraft being subjected to a Cold Proof Load Test (CPLT).

Strains were measured in Panel I and local sub-structure, on both the side of the aircraft where Panel I was installed and the opposite side of the aircraft, during cool-down and the CPLT. This report describes the thermal data and the correlation of strains with predictions made by the F-111 Internal Loads Model (ILM).

Strains beyond simple thermal contraction were generated during the cool-down from ambient to the CPLT test temperature of –40 °C because the airframe was manufactured from a range of materials with differing coefficients of thermal expansion (CTEs). These strains were moderate, up to approximately 450 με, and the difference between the sides of the aircraft with Panel I and the opposite side was typically less than 50 με. In the CRPSS the absolute magnitude of strains in the local sub-structure were reduced on the side of the aircraft where Panel I was installed. It is uncertain whether this observation was specific to the temperature/panel location in the CRPSS or a general result. If the result is general then incorporating components of reduced CTE, such as CRPs, into complex structure built-up from materials with higher CTE, such as metallic airframes, will reduce the magnitude of any thermally induced strains. Further testing is required at elevated temperature to validate this hypothesis.

The strains recorded in the CRPSS were compared to predictions made using the December 2002 version of the ILM and the fine grid sub-model. The measured strains matched predictions with a slightly inferior level of accuracy than the F-111C Fuselage Strain Survey. In particular the magnitude of strains in 12B-3945 Skin were over-predicted, probably because the joints between skin panels and sub-structure were excessively stiff. The FE models were not reworked to simulate more accurately this behaviour. Further work is therefore required to demonstrate conclusively that the combined effect of sub-ambient temperature and applied mechanical load on the strain in a F-111 airframe containing a CRP can be predicted with good accuracy.

5. References

1. Harman, A. B. and Callus, P. J., "Structural Analyses of a Demonstrator Composite Replacement Panel in a F-111C Cold Proof Load Test", Defence Science and Technology Organisation, Technical Note, DSTO-TN-0546, March 2004, 89 pp.
2. Callus, P. J., "Composite Replacement Panel Strain Survey (CRPSS) – Test Plan", Defence Science and Technology Organisation, Technical Note, DSTO-TN-0550, July 2004, 29 pp.
3. Sridhar, V. and Semple, B., "Correlation of F-111C ILM against A8-144 strain survey data", Engineering Report ER-F111-51-APM177, Aerostructures, Level 14, 222 Kingsway, South Melbourne, Victoria, 3207, Australia, 18 Jun 2004, 232 pp.
4. Fortburn Pty Ltd, "F-111C Aircraft, Serial Number A8-143, Strain gauge installation", Reference Number CRPSS F04-381, Fortburn Pty Ltd, 23 Rocklea Drive, Port Melbourne, Victoria, 3207, Australia, 29 June 2004, 16 pp.

5. Parkhill, G., "F-111C Panel 3208, Composite Replacement Panel Strain Survey, Data acquisition system and Cold Proof Load Test (CPLT) data", Report number P0410, PraxSys Pty Ltd, 18 Erskine Avenue, Cheltenham, Victoria, 3192, Australia, 14 July 2004, 24 pp.
6. Aerostructures, "F-111C Fuselage Strain Survey, Strain gauge locations, …" Engineering Drawings, ED-F111-51-APM 451, 452,457, 458, 459, 462,465, 489, Aerostructures, Level 14, 222 Kingsway, South Melbourne, Victoria, 3207, Australia, April and August 2001.

Appendix A: Data Analysis

The steps detailed in this Appendix were used to process and assess the data for each of the strain gauges in the CRPSS for each CPLT loadcase. The descriptors shown with the first letter in capitals (for example Elements, Show, Attributes and Elem Nodes) were the Patran commands that were used in executing the indicated processes.

A.1. Identified ILMr1 element number corresponding to gauge location

The ILMr1 model was opened in Patran. The digital images supplied with reference [4] and the transformation described in Section 3.1 were used to identify the element number(s) corresponding to each of the gauges. If gauges were located at the intersection of elements then the data from all the applicable elements was averaged.

A.2. Identified element surface on which strain gauge was bonded

The notation shown in Figure A1 was used to establish the element surface on which to interrogate for strain data. The element normal was identified using the "right hand thumb rule". The fingers of the right hand were circulated around the element in the order that the nodes appeared in the Node Locations dialog box (obtained using Elements, Show, Element, Attributes, Elem Nodes). The element normal was in the direction of the thumb.

The appropriate surface, Z1, Z2 or mid plane (equal to the average of Z1 and Z2), was selected depending on the position of the gauge on the real structure.

A.3. Identified strain gauge type

Uniaxial gauges were denoted "u". Rosettes were denoted as "abc" or "cba" depending on the relative position of the legs. The orientation was the order of the legs as determined with the right hand rule and the element normal as the positive z-axis. The two options are shown in Figure A2.

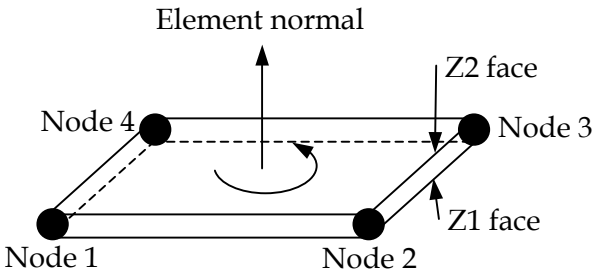

Figure A1: Diagram of an element showing the nodes, surfaces and normal (after reference [3])

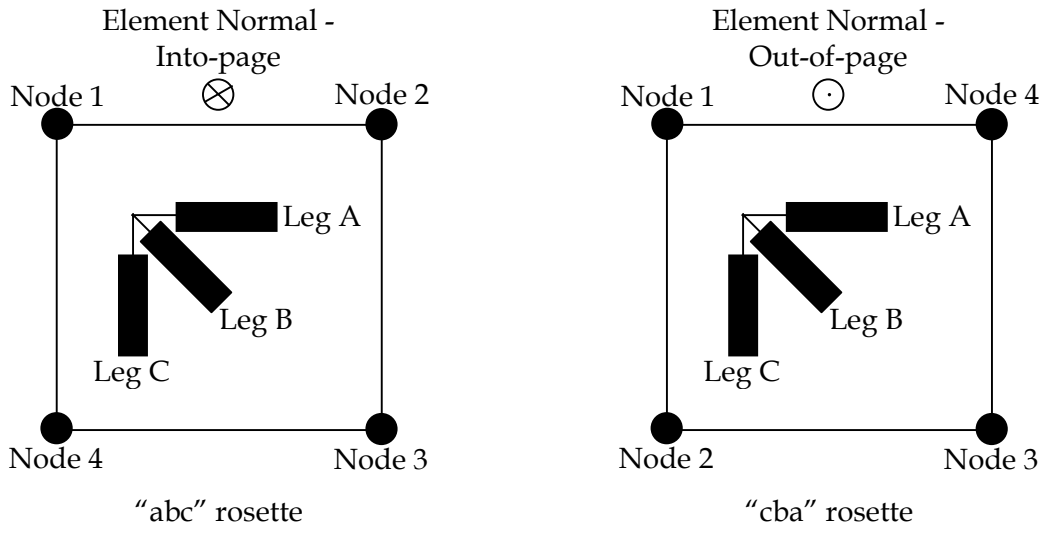

Figure A2: Plan views of elements showing the strain gauge orientation nomenclature

A.4. Identified strain gauge alignment (αa) relative to the element material axis

The following procedure was used:
Identified the Material Orientation (MCID) from the Show Element Properties dialog box (Elements, Show, Element, Attributes, Elem Props)
Displayed the Material Orientation (Display, Coordinate Frames, highlight Material Orientation, Post, OK)
Created Curve c that was parallel to the x-axis of the displayed MCID using:

Geometry, Create, Point, XYZ, Point ID nnn, Points Coordinate List [xxx yyy zzz]. Chose xxx, yyy and zzz to be a point on the element, typically the coordinates of a corner node (shown in Show Node Location Information dialog box from Elements, Show, Node, Location, single click on node) such that a linesubtended in the direction of the MCID x-axis could be projected onto the element surface.

Geometry, Create, Point, XYZ, Point ID nnn', [xxx' yyy' zzz']. Chose xxx', yyy' and zzz' to be a point on the MCID x-axis, approximately at the opposite end of the element from Point ID nnn.

Geometry, Create, Curve, Point, Curve ID c, Starting Point List nnn, Ending Point List nnn', Apply.

Created surface s that was parallel to the plane of the element using:

Identified the node number of the verticies of the region to be considered, v, vv, vvv, vvvv. Typically these were the four corner nodes on the element(s) that the gauge was bonded. Data for the nodes was shown in the Show Node Location Information dialog box (shown in Show Node Location Information dialog box from Elements, Show, Node, Location, click on node).

Geometry, Create, Surface, Vertex, Surface ID List s, Surface Vertex 1 List node v, Surface Vertex 2 List node vv, Surface Vertex 3 List node vvv, Surface Vertex 4 List node vvvv, Apply.

Created curve cc by projecting the x-axis of the MCID (curve c) onto the surface of the element (surface s) using:

Geometry, Create, Curve, Project, Curve ID cc, Option Normal to Surf, Curve List Curve c, Surface List Surf s, Apply

Created curve ccc parallel to the edge of the strain gauge using:

Geometry, Create, Curve, Project, Curve ID ccc, Starting Point List Point pp, Ending Point List Point ppp, Apply. Typically the gauges were parallel to the edge of elements and so pp and ppp were simply the appropriate corner nodes. If these were not parallel to the gauge then the appropriate locations were chosen.

Calculated the misalignment angle using:

Geometry, Show, Curve, Angle, First Curve List Curve cc, Second Curve List Curve ccc, Apply

The resulting angle was αa in degrees, αb = αa +45°, αc = αa + 90°

The misalignment angle was constrained between 0 and –180° for uniaxial gauges and –179 to 180° for rosettes. The angles were calculated using the x-axis of the MCID, element normal and the right hand rule, as shown in Figure A3.

A.5. Extracted the predicted strains

Viewed predictions in Patran using:

Results, Create, Fringe,

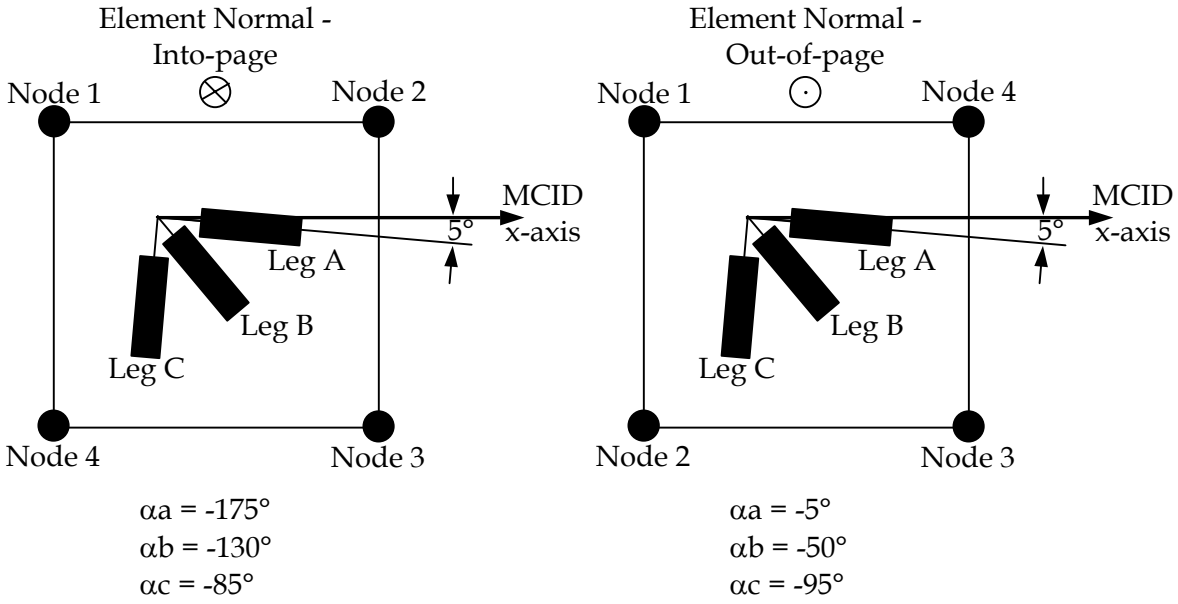

Figure A3: Plan views of elements showing the strain gauge alignment nomenclature

Select Results,

Select Results Case: (select each CPLT loadcase in turn), Select Fringe Result: Strain Tensor, Positions: Z1, Z2, Z1 and Z2 or layer 1 as appropriate, Quantity: obtained the X Component (εx), Y Component (εy), XY Engr Component (γxy), Max Principal 2D (εmax), Min Principal 2D (εmin) and Max Shear 2D (γxymax) for each CPLT loadcase.

Target Entities,

Target Entity: Elements, Select Elements: Elm (element number(s) on which the strain gauge was bonded).

Display Attributes,

Style: Element Fill, Display: Element Edges, Label Style: Integer.

Plot Options,

Coordinate Transformation: Material, Scale Factor: 1e+6 (so that results were in microstrain), Filter Values: None, Averaging Definition Domain: None, Method: Derive/Average, Extrapolation: Centroid.

A.6. Transformed predicted strains from material to strain gauge orientation

Equation A1 was used for uniaxial gauges and Equations A1, A2 and A3 for rosettes

$$\varepsilon a' = \varepsilon x \cos^2 \alpha a + \varepsilon y \sin^2 \alpha a + \gamma xy \sin \alpha a \cos \alpha a \quad \text{(A1)}$$

$$\varepsilon b' = \varepsilon x \cos^2 \alpha b + \varepsilon y \sin^2 \alpha b + \gamma xy \sin \alpha b \cos \alpha b \quad \text{(A2)}$$

$$\varepsilon c' = \varepsilon x \cos^2 \alpha c + \varepsilon y \sin^2 \alpha c + \gamma xy \sin \alpha c \cos \alpha c \quad \text{(A3)}$$

where:

$\varepsilon a'$ = component of strain in the direction of strain gauge Leg A
$\varepsilon b'$ = component of strain in the direction of strain gauge Leg B
$\varepsilon c'$ = component of strain in the direction of strain gauge Leg C
εx = strain in material x-axis
εy = strain in material y-axis
γxy = shear strain in material xy-plane
αa = angle between the material x-axis and strain gauge Leg A
αb = angle between the material x-axis and strain gauge Leg B
αc = angle between the material x-axis and strain gauge Leg C

A.7. Extracted CRPSS strains

As described in reference [5], data from the CRPSS was supplied as text files. These text files were downloaded into Excel spreadsheets and manipulated. The filenames were:

CRPSS_A8-143_CPLT100%_-2.40g_56°_Test_(Scan,Eng,ToFile)_0.txt
CRPSS_A8-143_CPLT100%_+7.33g_56°_Test_(Scan,Eng,ToFile)_0.txt
CRPSS_A8-143_CPLT100%_-3.00g_26°_Test_(Scan,Eng,ToFile)_0.txt
CRPSS_A8-143_CPLT100%_+7.33g_26°_Test_(Scan,Eng,ToFile)_0.txt

Progress through each CLT loadcase was recorded in terms of the consolidated load level. This was an averaged percentage of maximum load in a number of the load cell control channels. The strains quoted in this report were calculated as the averaged strain at zero consolidated load level subtracted from the averaged strain at the indicated consolidated load level. Peak strains were determined by averaging all data at the peak consolidated load level (100.1 % in the data files) then subtracting the averaged zero consolidated load level strain.

One of the columns in the data spreadsheets was an event marker. The event marker was triggered when the data acquisition operator activated a switch on the data acquisition console. This was done during the CRPSS to mark periods of particular interest. The marker was used immediately prior to the commencement of loading (zero load level) then at 20, 40, 60, 80, 100 and 0 % of the consolidated load level. The event marked data was not used, except for the zero load level, because during load holds the consolidated load level were maintained for longer than the event markers. Selecting the event marked data only would artificially reduce the data set. However, the strains at zero load were calculated as the average of the event marked strains immediately prior to the test.

A.8. Identified details of FSS strain gauges with a corresponding CRPSS gauge

The location of strain gauges in the CRPSS was chosen to be the same as that of corresponding gauges from the FSS.

The FSS gauge designations were established from reference [6].

Element numbers were obtained from reference [3].

Strain predictions from the ILM (denoted transformed ILM/SLIM predictions) and experimental data from the FSS were obtained from the Excel spreadsheet "Strain_comp_final.xls" specified in reference [3].

DISTRIBUTION LIST

Composite Replacement Panel Strain Survey – Test results and data analysis

Paul J. Callus

AUSTRALIA

DEFENCE ORGANISATION	**No. of copies**
Task Sponsor	
DGTA	1
S&T Program	
Chief Defence Scientist FAS Science Policy AS Science Corporate Management Director General Science Policy Development	Shared
Counsellor Defence Science, London	Doc Data Sheet
Counsellor Defence Science, Washington	Doc Data Sheet
Scientific Adviser to MRDC, Thailand	Doc Data Sheet
Scientific Adviser Joint	1
Navy Scientific Adviser	Doc Data Sht & Dist List
Scientific Adviser – Army	Doc Data Sht & Dist List
Air Force Scientific Adviser	1
Scientific Adviser to the DMO M&A	Doc Data Sht & Dist List
Platforms Sciences Laboratory	
Director of PSL (Corporate Leader Air)	Doc Data Sht & Exec Summ
Chief of Air Vehicles Division	Doc Data Sht & Dist List
Research Leader	Doc Data Sht & Dist List
Head	1
Task Manager	1
Author(s):	1
DSTO Library and Archives	
Library Fishermans Bend	Doc Data Sheet
Library Edinburgh	1
Defence Archives	1
Capability Development Group	
Director General Maritime Development	Doc Data Sheet
Director General Capability and Plans	Doc Data Sheet
Assistant Secretary Investment Analysis	Doc Data Sheet

Director Capability Plans and Programming	Doc Data Sheet
Director Trials	Doc Data Sheet

Chief Information Officer Group

Deputy CIO	Doc Data Sheet
Director General Information Policy and Plans	Doc Data Sheet
AS Information Strategy and Futures	Doc Data Sheet
AS Information Architecture and Management	Doc Data Sheet
Director General Australian Defence Simulation Office	Doc Data Sheet
Director General Information Services	Doc Data Sheet

Strategy Group

Director General Military Strategy	Doc Data Sheet
Director General Preparedness (delete "Doc Data Sheet" if a copy should be sent)	Doc Data Sheet
Assistant Secretary Governance and Counter-Proliferation	Doc Data Sheet

Navy

Maritime Operational Analysis Centre, Building 89/90 Garden Island Sydney NSW Deputy Director (Operations) Deputy Director (Analysis)	Doc Data Sht & Dist List
Director General Navy Capability, Performance and Plans, Navy Headquarters	Doc Data Sheet
Director General Navy Strategic Policy and Futures, Navy Headquarters	Doc Data Sheet

Air Force

SO (Science) - Headquarters Air Combat Group, RAAF Base, Williamtown NSW 2314	Doc Data Sht & Exec Summ

Army

ABCA National Standardisation Officer Land Warfare Development Sector, Puckapunyal	e-mailed Doc Data Sheet
SO (Science) - Land Headquarters (LHQ), Victoria Barracks NSW	Doc Data & Exec Summary
SO (Science), Deployable Joint Force Headquarters (DJFHQ) (L), Enoggera QLD	Doc Data Sheet

Joint Operations Command

Director General Joint Operations	Doc Data Sheet
Chief of Staff Headquarters Joint Operations Command	Doc Data Sheet
Commandant ADF Warfare Centre	Doc Data Sheet
Director General Strategic Logistics	Doc Data Sheet

Intelligence and Security Group

DGSTA Defence Intelligence Organisation	1
Manager, Information Centre, Defence Intelligence Organisation	1 (PDF)
Assistant Secretary Capability Provisioning	Doc Data Sheet
Assistant Secretary Capability and Systems	Doc Data Sheet
Assistant Secretary Corporate, Defence Imagery and Geospatial	Doc Data Sheet

Organisation	
Defence Materiel Organisation	
Deputy CEO	Doc Data Sheet
Head Aerospace Systems Division	Doc Data Sheet
Head Maritime Systems Division	Doc Data Sheet
Chief Joint Logistics Command	Doc Data Sheet
Defence Libraries	
Library Manager, DLS-Canberra	Doc Data Sheet
OTHER ORGANISATIONS	
National Library of Australia	1
NASA (Canberra)	1
Library of New South Wales	1
State Library of South Australia	1
UNIVERSITIES AND COLLEGES	
Australian Defence Force Academy	
Library	1
Head of Aerospace and Mechanical Engineering	1
Serials Section (M list), Deakin University Library, Geelong, VIC	1
Hargrave Library, Monash University	Doc Data Sheet
Librarian, Flinders University	1
OUTSIDE AUSTRALIA	
INTERNATIONAL DEFENCE INFORMATION CENTRES	
US Defense Technical Information Center	1 PDF
UK Dstl Knowledge Services	2
Canada Defence Research Directorate R&D Knowledge & Information Management (DRDKIM)	1
NZ Defence Information Centre	1
ABSTRACTING AND INFORMATION ORGANISATIONS	
Library, Chemical Abstracts Reference Service	1
Engineering Societies Library, US	1
Materials Information, Cambridge Scientific Abstracts, US	1
Documents Librarian, The Center for Research Libraries, US	1
INFORMATION EXCHANGE AGREEMENT PARTNERS	
National Aerospace Laboratory, Japan	1
National Aerospace Laboratory, Netherlands	1
SPARES	5

Total number of copies: 35 Printed: 33 PDF: 2

DEFENCE SCIENCE AND TECHNOLOGY ORGANISATION
DOCUMENT CONTROL DATA

1. PRIVACY MARKING/CAVEAT (OF DOCUMENT)

2. TITLE

Composite Replacement Panel Strain Survey – Test results and data analysis

3. SECURITY CLASSIFICATION (FOR UNCLASSIFIED REPORTS THAT ARE LIMITED RELEASE USE (L) NEXT TO DOCUMENT CLASSIFICATION)

Document	(U)
Title	(U)
Abstract	(U)

4. AUTHOR

Paul J. Callus

5. CORPORATE AUTHOR

Platforms Sciences Laboratory
506 Lorimer St
Fishermans Bend Victoria 3207 Australia

6a. DSTO NUMBER	6b. AR NUMBER	6c. TYPE OF REPORT	7. DOCUMENT DATE
DTSO-TR-1701	AR-013-373	Technical Report	April 2005

8. FILE NUMBER	9. TASK NUMBER	10. TASK SPONSOR	11. NO. OF PAGES	12. NO. OF REFERENCES
2004/1090908/1	AIR 03/188	DGTA	40	6

13. DOWNGRADING/DELIMITING INSTRUCTIONS

To be reviewed three years after date of publication

14. RELEASE AUTHORITY

Chief, Air Vehicles Division

15. SECONDARY RELEASE STATEMENT OF THIS DOCUMENT

Approved for public release

OVERSEAS ENQUIRIES OUTSIDE STATED LIMITATIONS SHOULD BE REFERRED THROUGH DOCUMENT EXCHANGE, PO BOX 1500, EDINBURGH, SA 5111

16. DELIBERATE ANNOUNCEMENT

No limitations

17. CITATION IN OTHER DOCUMENTS Yes

18. DEFTEST DESCRIPTORS

Composite replacement panel; F-111C aircraft; Airframe sub-structures; Strain gauge measurements, Free term: Finite Element Model

19. ABSTRACT

DSTO, in collaboration with the Cooperative Research Centre for Advanced Composite Structures, produced a demonstrator Composite Replacement Panel (CRP) as a replacement for F-111C Panel 3208 (Part Number 12B-3913). As part of the airworthiness certification program for the CRP technology, the demonstrator CRP, in the Composite Replacement Panel Strain Survey (CRPSS), was installed on a Royal Australian Air Force F-111C aircraft prior to a Cold Proof Load Test (CPLT). Strains in the CRP and local sub-structure were recorded as the aircraft was cooled from ambient to –40 °C. The magnitude of these thermally induced strains were moderate and lower on the side of the aircraft containing the CRP, implying that installing CRPs may reduce load in airframe sub-structures. The strain gauge measurements during the CPLT were compared with predictions made using the F-111C Internal Loads Finite Element Model and associated sub-models. The response of most strain gauges were predicted with reasonable accuracy although the strains in skin panels were not predicted well. Modification of the sub-models would be required to predict accurately the strains in all CRPSS gauges.